Efficient and Reliable Nonlocal Damage Models

A. Rodríguez-Ferran
I. Morata
A. Huerta

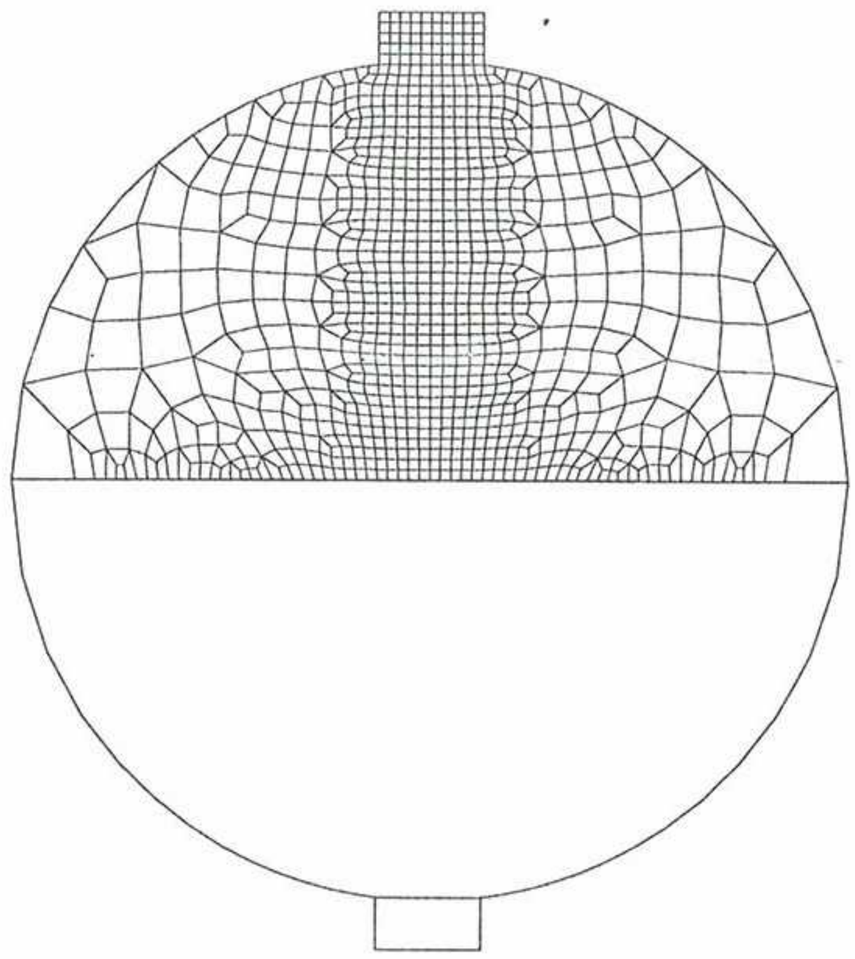

Publication CIMNE Nº-231, July 2003

Efficient and Reliable Nonlocal Damage Models

A. Rodríguez-Ferran
I. Morata
A. Huerta

Publication CIMNE Nº-231, July 2003

International Center for Numerical Methods in Engineering
Gran Capitán s/n, 08034 Barcelona, Spain

Efficient and Reliable Nonlocal Damage Models *

A. Rodríguez-Ferran *, I. Morata and A. Huerta

Laboratori de Càlcul Numèric (LaCàN), Universitat Politècnica de Catalunya, E-08034 Barcelona, Spain.

Abstract

We present an efficient and reliable approach for the numerical modelling of failure with nonlocal damage models. The two major numerical challenges – the strongly nonlinear, highly localized and parameter-dependent structural response of quasi-brittle materials, and the interaction between non-adjacent finite elements associated to nonlocality – are addressed in detail. Efficiency is achieved with a suitable combination of load-stepping control technique and nonlinear solver for equilibrium equations. Reliability of the numerical results is ensured by an h-adaptive strategy based on error estimation. We use a residual-type error estimator for nonlinear FE analysis based on local computations, which, at the same time, accounts for the nonlocality of the damage model. The proposed approach is illustrated by means of three application examples: the three-point bending test, the single-edge notched beam test and the Brazilian test. In addition, we present a new nonlocal damage model based on nonlocal displacements. Its good qualitative behaviour and attractive numerical properties are discussed and illustrated by means of a uniaxial tension test.

Key words: quasi-brittle materials; nonlocal damage models; adaptivity; error estimation; consistent tangent matrix; quadratic convergence; nonlocal displacements

* Research supported by Ministerio de Ciencia y Tecnología under grant DPI2001-2204

* Correspondence to: Antonio Rodríguez-Ferran, Departament de Matemàtica Aplicada III, E.T.S. de Ingenieros de Caminos, Canales y Puertos, Universitat Politècnica de Catalunya, Jordi Girona 1, E-08034 Barcelona, SPAIN.

Email address: antonio.rodriguez-ferran@upc.es (A. Rodríguez-Ferran).

URL: www-lacan.upc.es (A. Rodríguez-Ferran).

1 Introduction

Damage models are nowadays a common choice in the numerical modelling of failure of quasi-brittle materials [1]. To avoid the pathological mesh dependence exhibited by local damage models, one may use either gradient damage models or nonlocal damage models. These two related strategies regularize the problem and ensure mesh objectivity. In gradient damage models, strain derivatives are incorporated into the constitutive equation [2]. In nonlocal damage models [3,4,5], strain (or, rather, a strain-related state variable) is smoothed by means of an integral average in the vicinity – associated to a characteristic length – of each point. The latter approach is considered in this paper.

Another clear trend in computational mechanics is the quest for reliable computations. The quality of the results must be guaranteed in an quantifiable, objective manner. This has led to adaptive finite element analysis based on error estimation.

The price to pay for reliable results is a large number of degrees of freedom, especially in nonlinear solid mechanics. This means that one needs computationally efficient numerical methods.

Of course, efficiency and reliability is a general concern in all the fields of computational mechanics. However, when modelling quasi-brittle failure with nonlocal damage models, we face some specific challenges:

(1) Due to brittleness, the structural response is strongly nonlinear, very localized and highly dependent (at the quantitative and even qualitative level) on the value of the material parameters.
(2) Due to nonlocality, there is interaction between non-adjacent finite elements. This poses several difficulties. The consistent tangent stiffness matrix, for instance (needed for quadratic convergence in Newton iterations), cannot be assembled from elementary contributions solely.
(3) Many error estimators are based on local (element-wise) computations. This fact must be conciliated with the nonlocal nature of the damage model: adaptivity typically leads to element sizes smaller than characteristic length.

1.1 Objectives

In this context, the main goal of this paper is to present an efficient and reliable approach for the numerical modelling of failure with nonlocal damage models. The key ingredients are:

(1) A residual-type error estimator based on element-wise computations which, at the same time, accounts for the nonlocality of the constitutive model [6].
(2) An h-adaptive strategy driven by the error estimator which yields numerical results with the desired accuracy. The FE discretization errors are kept under control and, thus, the physical significance of the computations is guaranteed [7,6].
(3) Advanced arc-length control techniques, adapted to the highly localized failure patterns.
(4) A flexible approach to achieve quadratic convergence in Newton iterations. The element-to-element stiffness matrices can either be assembled into the global tangent stiffness matrix [8] or accounted for in the right-hand-side vector to prevent fill-in.

This paper also addresses another issue: the use of nonlocal *displacements* as the basis of the nonlocal damage model. The standard approach is to define the nonlocal state variable as the nonlocal average (NLA) of the (strain-related) local state variable. Other approaches have been proposed in the literature (see [9] for a comparative analysis), based, for instance, on nonlocal strains or nonlocal damage. An alternative approach is presented here: to use nonlocal displacements, obtained as the NLA of local displacements, to drive the evolution of damage. According to our preliminary numerical experiments, the resulting model exhibits a satisfactory behaviour and it is very attractive from the computational point of view, especially regarding the computation of the consistent tangent matrix.

1.2 Outline of Paper

The rest of the paper is organized as follows. Nonlocal damage models are briefly reviewed in Sect. 2. The proposed model based on nonlocal displacements is presented in Sect. 3. Numerical aspects are discussed in Sect. 4. Although they are clearly interrelated, the issues of efficiency and reliability are covered separately for expository purposes. Regarding efficiency, see Sect. 4.1, the key features are adequate control strategies (for load-stepping) and iterative solvers (for iterations within the load-step). The consistent tangent matrix for the proposed model based on nonlocal displacements is derived in Sect. 4.1.4. Reliability, see Sect. 4.2, refers to the adaptive strategy based on error estimation. The two main aspects, nonlinearity and nonlocality, are covered respectively in Sects. 4.2.1 and 4.2.2. Section 5 contains some illustrative applications. Finally, the concluding remarks of Sect. 6 close the paper.

Table 1
General expression of an elastic-damage model

Stress-strain relationship	$\boldsymbol{\sigma}(\mathbf{x},t) = \big(1 - D(\mathbf{x},t)\big)\,\mathbf{C}\boldsymbol{\varepsilon}(\mathbf{x},t)$	(1)
Local state variable	$Y(\mathbf{x},t) = Y\big(\boldsymbol{\varepsilon}(\mathbf{x},t)\big)$	(2)
Nonlocal state variable	$\widetilde{Y}(\mathbf{x},t) = \int_{V_x} \alpha(\mathbf{x}-\mathbf{z}) Y(\mathbf{z},t)\,\mathrm{d}V$	(3)
Weighting function	$\alpha(\mathbf{x}-\mathbf{z}) = \alpha(r; l_\mathrm{c})$ with $r = \|\mathbf{x}-\mathbf{z}\|$	(4)
Damage evolution	$D(\mathbf{x},t) = D\big(\max_{\tau \le t} \widetilde{Y}(\mathbf{x},\tau)\big)$	(5)

2 Overview of Nonlocal Damage Models

For simplicity, only elastic-scalar damage models are considered here. However, many of the ideas, methods and algorithms can be extended to more complex damage models incorporating, for instance, anisotropy or plasticity [5,10].

A generic nonlocal model of such type consists of the following equations, summarized in Table 1:

- A relation between Cauchy stresses $\boldsymbol{\sigma}$ and small strains $\boldsymbol{\varepsilon}$, where the loss of stiffness (from elastic stiffness $\mathbf{C}$ to zero stiffness) is described by means of a scalar damage parameter D which ranges from 0 to 1, (1);
- The definition of a local state variable Y as a function of strain $\boldsymbol{\varepsilon}$, (2);
- The definition of the nonlocal state variable $\widetilde{Y}$ as the average of the local state variable Y, (3);
- A weighting function α which depends on the distance r between two points and contains a characteristic length l_c as a parameter, (4);
- A damage evolution law, where the nonlocal state variable $\widetilde{Y}$ drives the evolution of the non-decreasing damage parameter D, (5).

Many nonlocal damage models encountered in the literature can be accommodated with little or no modification into the general framework of Table 1. The most common choices for (2), (4) and (5) are reviewed next.

2.1 Local State Variable

The local state variable Y is a suitable scalar measure of strains $\boldsymbol{\varepsilon}$. Three common definitions are the energy release rate [1,11]

$$Y = \frac{1}{2}\boldsymbol{\varepsilon}^T \mathbf{C}\boldsymbol{\varepsilon}\,, \tag{6}$$

the average of positive principal strains ε_i used in the Mazars model [12]

$$Y = \sqrt{\sum_i \left[\max(0, \varepsilon_i)\right]^2}\,, \tag{7}$$

and a function of strain invariants used in the modified von Mises model [13]

$$Y = \frac{k-1}{2k(1-2\nu)} I_1 + \frac{1}{2k}\sqrt{\left(\frac{k-1}{1-2\nu} I_1\right)^2 + \frac{12k}{(1+\nu)^2} J_2}\,. \tag{8}$$

In (8), I_1 and J_2 are the first and second invariants of the strain and deviatoric strain tensors respectively, and k is the ratio of compressive to tensile strength.

2.2 Weighting Function

The weighting function α is typically defined as

$$\alpha(r; l_c) = \frac{\alpha_0(r; l_c)}{\int_{V_x} \alpha_0(r; l_c)\, \mathrm{d}V} \tag{9}$$

where α_0 is the Gaussian function [14,15,7]

$$\alpha_0(r; l_c) = \exp\left[-\left(\frac{2r}{l_c}\right)^2\right]\,. \tag{10}$$

For computational efficiency, the infinite support of the Gaussian function is truncated for the nonlocal averaging. Another possibility is to use a parabolic function with compact support, see [9]. In any case, the integral in the denominator of (9) is not a constant: near the boundaries, the support of α_0 may lay partially outside the domain, so a lower value of the integral is obtained. In fact, it is necessary to modify the Gaussian function α_0 into the weighting function α as indicated by (9) to ensure *consistency of order 0* (i.e. reproducibility of constant functions). This guarantees that a constant field of local state variable $Y(\mathbf{x}) = Y$ is not modified due to nonlocal averaging (that is, $\widetilde{Y}(\mathbf{x}) = Y(\mathbf{x}) = Y$) and, hence, that a constant strain field $\boldsymbol{\varepsilon}$ results in a constant stress field $\boldsymbol{\sigma}$.

As a remark, is is worth noting that this function is sometimes written as [9,16]

$$\alpha_0(r; l_c) = \exp\left[-\left(\frac{r}{\sqrt{2} l_c}\right)^2\right]\,. \tag{11}$$

Note that the characteristic lengths in (10) and (11) differ by a factor of $2\sqrt{2}$.

2.3 *Damage Evolution Law*

Two typical choices to describe the evolution of damage above the damage threshold Y_0 are the exponential law [12]

$$D = 1 - \frac{Y_0(1-A)}{\widetilde{Y}} - A\exp\left[-B\left(\widetilde{Y} - Y_0\right)\right] \tag{12}$$

and the polynomial law [17,16]

$$D = 1 - \frac{1}{1 + B(\widetilde{Y} - Y_0) + A(\widetilde{Y} - Y_0)^2}\,. \tag{13}$$

In (12) and (13), parameter A is associated to residual strength and parameter B controls the slope of the softening branch at the peak (i.e. at $\widetilde{Y} = Y_0$), see [7].

In Mazars model, damage D is expressed as a combination of tensile damage D_t and compressive damage D_c [12]. Each of these two components evolves according to an exponential law (12), with the corresponding parameters A_c and B_c for compression and A_t and B_t for tension.

3 A Nonlocal Damage Model Based on Nonlocal Displacements

As Table 1 reflects, the standard approach is to define a scalar local state variable Y (as a function of strains) and then to average it into the nonlocal state variable $\widetilde{Y}$, which drives the evolution of damage.

However, other variables can be selected for averaging. In fact, a number a proposals can be found in the literature. Either scalar (for instance: damage D) or vectorial (for instance: strain $\boldsymbol{\varepsilon}$) Gauss-point quantities may be averaged into the corresponding nonlocal quantities ($\widetilde{D}$ and $\widetilde{\boldsymbol{\varepsilon}}$ in the two examples mentioned). The existing approaches are compared in [9] by means of a simple 1D numerical test (bar under uniaxial tension).

A new proposal is made here: to compute nonlocal displacements $\widetilde{\mathbf{u}}$ by averaging the local (i.e. standard) displacements $\mathbf{u}$. These nonlocal displacements $\widetilde{\mathbf{u}}$ drive the evolution of damage, see Table 2.

Regarding the basic ingredients of a nonlocal damage model reviewed in Sect. 2, the only one that requires some modification is the weighting function. Since displacements, rather than strains, are averaged, *consistency of order 1* (i.e.

Table 2
Standard approach (nonlocal state variable) vs. alternative approach (nonlocal displacements). Subscript NL denotes quantities with nonlocal information but computed locally. The tilde is reserved to truly nonlocal quantities (i.e. computed via nonlocal average, NLA, of a local quantity)

Standard approach	**Alternative approach**
Local displacement $\mathbf{u}$	Local displacement $\mathbf{u}$
Local strain $\boldsymbol{\varepsilon} = \nabla^s \mathbf{u}$	Nonlocal displacement $\widetilde{\mathbf{u}} = \mathrm{NLA}(\mathbf{u})$
Local state var. $Y = Y(\boldsymbol{\varepsilon})$	Nonlocal strain $\boldsymbol{\varepsilon}_{\mathrm{NL}} = \nabla^s \widetilde{\mathbf{u}}$
Nonlocal state var. $\widetilde{Y} = \mathrm{NLA}(Y)$	Nonlocal state var. $Y_{\mathrm{NL}} = Y(\boldsymbol{\varepsilon}_{\mathrm{NL}})$
Damage evolution $D = D(\widetilde{Y})$	Damage evolution $D = D(Y_{\mathrm{NL}})$
	Local strain $\boldsymbol{\varepsilon} = \nabla^s \mathbf{u}$
Stress-strain law $\boldsymbol{\sigma} = (1 - D)\mathbf{C} : \boldsymbol{\varepsilon}$	Stress-strain law $\boldsymbol{\sigma} = (1 - D)\mathbf{C} : \boldsymbol{\varepsilon}$

reproducibility of polynomials of degree 1) is needed to ensure that a constant strain field results in a constant stress field.

This can be achieved by means of a moving least-squares fitting, a standard technique in particle (or meshless) methods [18,19], briefly summarized here.

For a given point $\mathbf{x}$, the goal is to approximate a function f in the neighbourhood V_x (in our case, associated to a characteristic length) of $\mathbf{x}$ by means of a polynomial of degree n, $\mathbf{f}_{l_c}(\mathbf{z})$,

$$f_{l_c}(\mathbf{z}) = \mathbf{P}^T(\mathbf{z})\mathbf{c}(\mathbf{x}) \tag{14}$$

where $\mathbf{P}(\mathbf{z}) = \{p_0(\mathbf{z}), p_1(\mathbf{z}), \ldots, p_n(\mathbf{z})\}^T$ contains a complete basis of the space of polynomials of degree less or equal to n. The vector of coefficients $\mathbf{c}(\mathbf{x})$ is obtained by a least squares fitting with the local scalar product

$$\langle g, h \rangle_x = \int_{V_x} \alpha_0(\mathbf{x} - \boldsymbol{\xi}) g(\boldsymbol{\xi}) h(\boldsymbol{\xi}) \, \mathrm{d}\boldsymbol{\xi} \,, \tag{15}$$

centered at $\mathbf{x}$ and weighted with α_0. The resulting normal equations are

$$\mathbf{M}(\mathbf{x})\mathbf{c}(\mathbf{x}) = \mathbf{b}(\mathbf{x}) \tag{16}$$

with

$$\mathbf{M}(\mathbf{x}) = \int_{V_x} \alpha_0(\mathbf{x} - \boldsymbol{\xi}) \mathbf{P}(\boldsymbol{\xi}) \mathbf{P}^T(\boldsymbol{\xi}) \, \mathrm{d}\boldsymbol{\xi} \tag{17}$$

and

$$\mathbf{b}(\mathbf{x}) = \int_{V_x} \alpha_0(\mathbf{x} - \boldsymbol{\xi}) \mathbf{P}(\boldsymbol{\xi}) f(\boldsymbol{\xi}) \, \mathrm{d}\boldsymbol{\xi} \,. \tag{18}$$

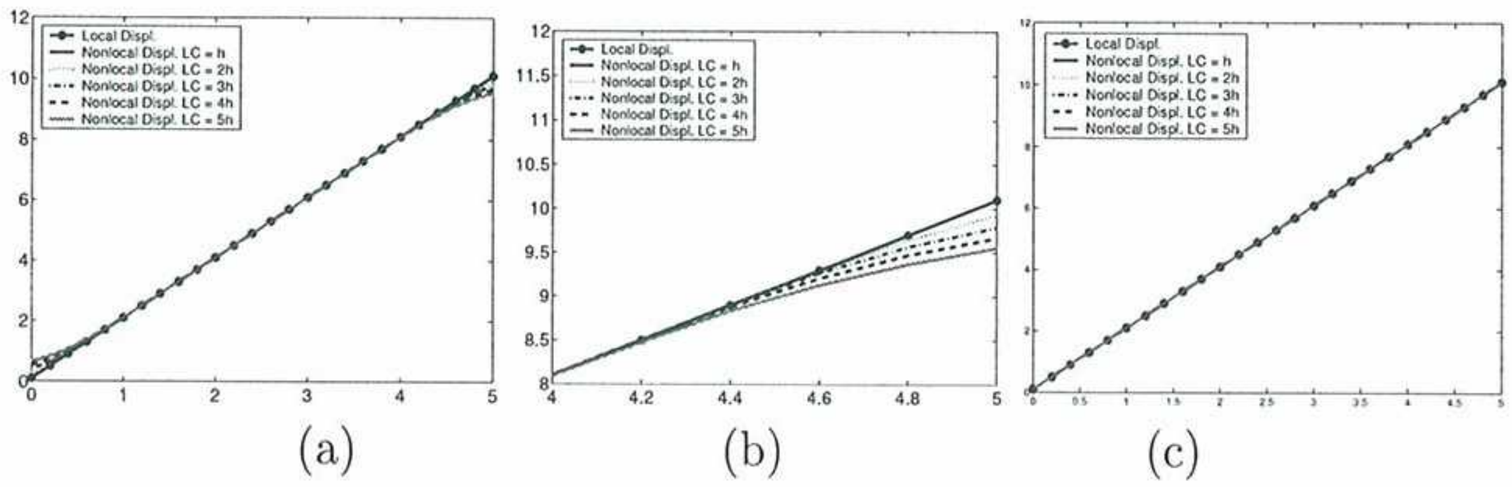

Figure 1. Nonlocal average of a linear function. Consistency of order 0: (**a**) whole domain; (**b**) zoom in boundary. (**c**) Consistency of order 1

The smoothed function at $\mathbf{x}$, $\widetilde{f}(\mathbf{x})$, is obtained by evaluating the local polynomial approximation (14) at $\mathbf{z} = \mathbf{x}$, that is

$$\widetilde{f}(\mathbf{x}) = f_{l_c}(\mathbf{z} = \mathbf{x}) = \mathbf{P}^T(\mathbf{x})\mathbf{c}(\mathbf{x})\,. \tag{19}$$

For $n = 0$ (consistency of order 0), (19) boils down to the standard nonlocal averaging represented by (3) and (9). For $n = 1$ (consistency of order 1), (16) is a linear system of dimension 2 to be solved at each node. This is done only once, at the beginning of the computation, and coefficients $c_0(\mathbf{x})$ and $c_1(\mathbf{x})$ are stored and reused throughout the analysis.

The relevance of consistency of order 1 is illustrated by Fig. 1. If a linear 1D field of local displacements is averaged with the weighting function (9), see Fig. 1(a), it is not reproduced correctly near the boundaries. The discrepancy increases with nonlocality, measured as the ratio of characteristic length to element size, see zoom in Fig. 1(b). With consistency of order 1, on the other hand, the nonlocal displacement field matches the local field, see Fig. 1(c).

4 Numerical Aspects

As discussed in the introduction, *reliability* and *efficiency* are the two major issues in virtually any branch of computational (solid and fluid) mechanics. When modelling quasi-brittle materials, the development of reliable and efficient algorithms must take into account that the structural response is typically (1) very nonlinear, (2) localized, (3) highly dependent on the value of material parameters and (4) geometrically complex (curved cracks, primary and secondary failure mechanisms, etc.).

4.1 Efficiency

Due to material nonlinearity, FE discretization of the equilibrium equation leads to a nonlinear system of algebraic equations, which is solved in an incremental-iterative fashion [20,21]. Thus, the two key ingredients for an efficient numerical model are:

(1) An adequate control strategy to define the increments (i.e. time- or load-stepping).
(2) A suitable nonlinear solver for the iterations within each increment, including the appropriate (secant or tangent) stiffness matrices.

4.1.1 Control Strategy (for Increments)

The softening behaviour of the stress-strain law leads to structural softening of the snap-through or snap-back type, as shown in Figs. 11, 20 and 26 of Sect. 5. As a consequence, force control is not a suitable control strategy; either displacement control (for snap-through) or arc-length control (for snap-through or snap-back) are required.

In any case, the localized nature of quasi-brittle failure must be accounted for. For arc-length control, for instance, the classical constraint [20]

$$\sqrt{\Delta\mathbf{u}^T\Delta\mathbf{u} + (\Delta\mathbf{f}^{\text{ext}})^T\Delta\mathbf{f}^{\text{ext}}} = \Delta s\,, \tag{20}$$

which prescribes the norm of the increment of solution (displacement and external forces) to a given arc-length Δs is not appropriate, because $\Delta\mathbf{u}$ is a global quantity that does not reflect localization.

Alternative constraints are required. Two possibilities are [7]

$$\max|\Delta\varepsilon_{ij}| = \Delta s \tag{21}$$

and

$$|\Delta u_{\text{characteristic}}| = \Delta s\,, \tag{22}$$

where $u_{\text{characteristic}}$ is one (or a combination of a few) characteristic degree(s) of freedom. For notched specimens, for instance, one can use the CMOD (Crack-Mouth Opening Displacement) or CMSD (Crack-Mouth Sliding Displacement) as the arc-length parameter.

Another important issue is the proper selection of the prescribed arc-length Δs. For complex computations, it is not practical to use a constant value, so automatic load-stepping is required to adapt the "load-step" Δs along the analysis. A common choice is to use ad-hoc formulas based on comparing the

desired number of iterations per step with the actual number of iterations in the last step [20].

A more rigorous approach is to use adaptive time-stepping strategies based on techniques for the numerical solution of ordinary differential equations. The time error is controlled such that it is at least one order of magnitude smaller than the space error. Thus, the effect of the time integration in the space error may be considered negligible. This approach is developed in [22] for initial boundary value problems (i.e. evolutionary problems involving, for instance, viscoelasticity or coupled chemo-mechanical behaviour of concrete). This idea makes even more sense for the boundary value problem under consideration here, where inertia effects are neglected (quasistatic problem), so physical time does not appear in the governing equations. If load steps (that is, pseudo-time increments) are properly chosen, then the error associated to load-stepping is negligible with respect to the space error for each load level.

4.1.2 Nonlinear Solver and Stiffness Matrix (for Iterations)

Within each increment, the equilibrium equation remains nonlinear and demands an iterative solution. A nonlinear solver amounts basically to the selection of a particular stiffness matrix.

One possibility [17,15,7,6] is to work with the secant stiffness matrix, computed from the damaged elastic moduli $(1-D)\mathbf{C}$. The main advantage of this approach is that the secant matrix is symmetric positive definite and very simple to compute (the factor $(1-D)$ at each Gauss point is the only difference with respect to the elastic stiffness matrix). The main drawback is that it must be supplemented with convergence acceleration and, even so, convergence is only linear.

If quadratic convergence is desired (full Newton-Raphson method), the consistent tangent matrix is required [21]. For nonlocal damage models, this poses a substantial difficulty: due to nonlocality, there is interaction between non-adjacent nodes, and the consistent tangent matrix exhibits a larger bandwidth (with respect to the sparsity pattern of the elastic or secant matrices) [17,8], as discussed next.

In FE analysis, the internal force vector is typically computed with a Gauss quadrature as

$$\mathbf{f}_{\text{int}}(\mathbf{u}) = \sum_p w_p \mathbf{B}_p^T \boldsymbol{\sigma}_p(\mathbf{u}) \tag{23}$$

where p ranges the Gauss points, w_p are the corresponding integration weights, $\mathbf{B}_p$ is the usual matrix of shape function derivatives at Gauss point p and

stresses $\boldsymbol{\sigma}_p$ are

$$\boldsymbol{\sigma}_p(\mathbf{u}) = (1 - D_p)\mathbf{C}\underbrace{\mathbf{B}_p\mathbf{u}}_{\boldsymbol{\varepsilon}_p} . \tag{24}$$

The consistent tangent matrix is

$$\mathbf{K}_{\text{tan}} := \frac{\partial \mathbf{f}_{\text{int}}}{\partial \mathbf{u}} = \sum_p w_p \mathbf{B}_p^T \frac{\partial \boldsymbol{\sigma}_p}{\partial \mathbf{u}} . \tag{25}$$

Combining (24) and (25) results in

$$\mathbf{K}_{\text{tan}} = \mathbf{K}_{\text{sec}} + \mathbf{K}_{\text{nonlocal}} \tag{26}$$

where

$$\mathbf{K}_{\text{sec}} = \sum_p w_p \mathbf{B}_p^T (1 - D_p)\mathbf{C}\mathbf{B}_p \tag{27}$$

is the secant stiffness matrix and

$$\mathbf{K}_{\text{nonlocal}} = -\sum_p w_p \mathbf{B}_p^T \mathbf{C}\boldsymbol{\varepsilon}_p \frac{\partial D_p}{\partial \mathbf{u}} \tag{28}$$

is the nonlocal tangent contribution which accounts for the variation of the damage parameter.

By applying the chain rule, the term $\partial D_p/\partial \mathbf{u}$ can be expressed as

$$\frac{\partial D_p}{\partial \mathbf{u}} = D'(\tilde{Y}_p)\frac{\partial \tilde{Y}_p}{\partial \mathbf{u}} . \tag{29}$$

The integral (3) required for nonlocal averaging is also approximated via a numerical quadrature, so the nonlocal state variable $\tilde{Y}_p$ is

$$\tilde{Y}_p = \sum_{q \in V_p} w_q \alpha_{pq} Y_q , \tag{30}$$

where q ranges the Gauss points $\boldsymbol{\xi}_q$ in the neighbourhood V_p of Gauss point $\boldsymbol{\xi}_p$, and $\alpha_{pq} = \alpha(r = \|\boldsymbol{\xi}_p - \boldsymbol{\xi}_q\|)$.

By differentiating (30), the last term in (29) can be expressed as

$$\frac{\partial \tilde{Y}_p}{\partial \mathbf{u}} = \sum_{q \in V_p} w_q \alpha_{pq} \frac{\partial Y_q}{\partial \mathbf{u}} = \sum_{q \in V_p} w_q \alpha_{pq} \frac{\partial Y_q}{\partial \boldsymbol{\varepsilon}} \mathbf{B}_q \tag{31}$$

where the chain rule and the relation $\partial \boldsymbol{\varepsilon}_q/\partial \mathbf{u} = \mathbf{B}_q$ have been used.

Table 3
Properties of stiffness matrices

Matrix		Symmetry	Increased bandwidth	Nonlocal interaction	Convergence
$\mathbf{K}_{\text{sec}}$	Secant	Yes	No	No	Linear
$\mathbf{K}_{\text{sec}} + \mathbf{K}_{\text{local},Y}$	Local tangent	No	No	No	Linear
$\mathbf{K}_{\text{tan}}$	Consistent tangent	No	Yes	Yes	Quadratic

By replacing (31) into (29) and then into (28), the nonlocal matrix can be expressed as

$$\mathbf{K}_{\text{nonlocal},Y} = -\sum_{p,q \in V_p} w_{pq} \mathbf{B}_p^T \mathbf{C} \boldsymbol{\varepsilon}_p D'(\tilde{Y}_p) \frac{\partial Y_q}{\partial \boldsymbol{\varepsilon}} \mathbf{B}_q \tag{32}$$

where $w_{pq} = w_p w_q \alpha_{pq}$ and the subscript Y denotes the nonlocal quantity. Due to the double loop in Gauss points caused by nonlocal interaction, $\mathbf{K}_{\text{nonlocal},Y}$ cannot be assembled from elementary contributions solely.

To avoid the additional non-zero entries, some authors [13,16] neglect the nonlocal interaction by taking $w_{pq} = 0$ for $p \neq q$:

$$\mathbf{K}_{\text{local},Y} = -\sum_{p} w_{pp} \mathbf{B}_p^T \mathbf{C} \boldsymbol{\varepsilon}_p D'(\tilde{Y}_p) \frac{\partial Y_p}{\partial \boldsymbol{\varepsilon}} \mathbf{B}_p \,. \tag{33}$$

However, the resulting local tangent matrix $\mathbf{K}_{\text{sec}} + \mathbf{K}_{\text{local},Y}$ is no longer consistent, and quadratic convergence is lost.

These three basic choices are summarized in Table 3.

4.1.3 Quadratic Convergence Without Fill-in

If the consistent tangent matrix is chosen, equilibrium iterations read

$$\mathbf{K}_{\text{tan}}^i \delta \mathbf{u}^{i+1} = -\mathbf{r}^i \,, \tag{34}$$

where i is the iteration counter, $\mathbf{r}^i$ is the residual and $\delta \mathbf{u}^{i+1}$ is the iterative correction in displacements.

Due to the increased bandwidth of $\mathbf{K}_{\text{tan}}^i$, fill-in during the factorization is considerably larger than for a local (tangent or secant) stiffness matrix. If this additional fill-in is a critical factor, it can be avoided by accounting for the nonlocal interaction in the right-hand-side vector. The consistent tangent matrix can be expressed as

$$\mathbf{K}_{\text{tan}} = \mathbf{K}_{\text{sec}} + \mathbf{K}_{\text{local},Y} + \mathbf{K}_{p \neq q, Y} \tag{35}$$

where $\mathbf{K}_{p\neq q,Y}$ is the part of the nonlocal matrix $\mathbf{K}_{\text{nonlocal},Y}$ neglected when approximating (32) by (33).

Equations (34) and (35) can be combined into the system of equations

$$\left(\mathbf{K}^i_{\text{sec}} + \mathbf{K}^i_{\text{local},Y}\right)\delta\mathbf{u}^{i+1} = -\mathbf{r}^i - \mathbf{K}^i_{p\neq q,Y}\delta\mathbf{u}^{i+1} \tag{36}$$

which can be solved with an inner iterative scheme,

$$\left(\mathbf{K}^i_{\text{sec}} + \mathbf{K}^i_{\text{local},Y}\right)\delta\mathbf{u}^{i+1}_{k+1} = -\mathbf{r}^i - \mathbf{K}^i_{p\neq q,Y}\delta\mathbf{u}^{i+1}_{k} \tag{37}$$

where k is the counter for the inner iterations. Note that extra fill-in is indeed precluded, because the matrix in system (37) is local. Moreover, once $\mathbf{K}^i_{\text{sec}} + \mathbf{K}^i_{\text{local},Y}$ is factorized, the inner iterations have a relatively modest computational cost. Linear convergence is expected for these inner iterations k, but – and this is the key issue –, quadratic convergence without increased fill-in will be achieved for the expensive, outer equilibrium equations i. Moreover, the tolerance of the inner k loop is usually not taken as a constant, but dependent on outer iteration i to increase the efficiency. This is standard in numerical algebra [23]. In fact at the initial iterations of the Newton-Raphson method a larger tolerance is prescribed and, as i increases, the tolerance of the inner loop approaches the standard value.

If factorizing the non-symmetric matrix $\mathbf{K}^i_{\text{sec}} + \mathbf{K}^i_{\text{local},Y}$ is inconvenient with the finite element code at hand, matrix $\mathbf{K}^i_{\text{local},Y}$ can be taken to the right-hand-side. The inner loop then reads

$$\mathbf{K}^i_{\text{sec}}\delta\mathbf{u}^{i+1}_{k+1} = -\mathbf{r}^i - K^i_{\text{nonlocal},Y}\delta\mathbf{u}^{i+1}_{k}\,, \tag{38}$$

and the usual Cholesky factorization applies. More (but cheaper) inner iterations should be expected.

4.1.4 Consistent tangent matrix for model based on nonlocal displacements

The proposed model based on nonlocal displacements has very attractive numerical properties. As shown here, the consistent tangent matrix is quite simpler to compute than in the standard case shown above.

Equations (23)-(28) are also valid for the new model. However, the term $\partial D_p/\partial\mathbf{u}$ is now

$$\frac{\partial D_p}{\partial\mathbf{u}} = D'(Y_{\text{NL}_p})\frac{\partial Y}{\partial\boldsymbol{\varepsilon}_{\text{NL}}}(\boldsymbol{\varepsilon}_{\text{NL}_p})\frac{\partial\boldsymbol{\varepsilon}_{\text{NL}_p}}{\partial\tilde{\mathbf{u}}}\frac{\partial\tilde{\mathbf{u}}}{\partial\mathbf{u}}\,. \tag{39}$$

Note that nonlocal strains $\boldsymbol{\varepsilon}_{\text{NL}}$ are computed *locally* as the symmetrized gra-

dient of nonlocal displacements, see Table 2. This means that

$$\varepsilon_{\mathrm{NL}_p} = \mathbf{B}_p \tilde{\mathbf{u}} \qquad \Longrightarrow \qquad \frac{\partial \varepsilon_{\mathrm{NL}_p}}{\partial \tilde{\mathbf{u}}} = \mathbf{B}_p \,. \tag{40}$$

The last term in (39), $\partial\tilde{\mathbf{u}}/\partial\mathbf{u}$, reflects the nonlocality of the model. After finite element discretization and numerical integration, the averaging process (19) leads simply to

$$\tilde{\mathbf{u}} = \mathbf{A}\mathbf{u} \qquad \Longrightarrow \qquad \frac{\partial \tilde{\mathbf{u}}}{\partial \mathbf{u}} = \mathbf{A} \,, \tag{41}$$

where $\mathbf{A}$ is a matrix of nonlocal connectivity. Note that this matrix contains purely geometrical information. It does not change as damage evolves, so it can be computed and stored at the beginning of the analysis.

Substitution of (39), (40) and (41) into (28) results in

$$\mathbf{K}_{\mathrm{nonlocal},\mathbf{u}} = \mathbf{K}_{\mathrm{local},\mathbf{u}} \mathbf{A} \tag{42}$$

with

$$\mathbf{K}_{\mathrm{local},\mathbf{u}} = -\sum_p w_p \mathbf{B}_p^T \mathbf{C} \boldsymbol{\varepsilon}_p D'(Y_{\mathrm{NL}_p}) \frac{\partial Y}{\partial \varepsilon_{\mathrm{NL}}}(\varepsilon_{\mathrm{NL}_p}) \mathbf{B}_p \,. \tag{43}$$

Note that $\mathbf{K}_{\mathrm{local},\mathbf{u}}$ can be computed in the usual way by assembling elementary matrices, like in any local material model. After that, nonlocality is accounted for by means of the constant matrix $\mathbf{A}$, which "spreads" the stiffness of $\mathbf{K}_{\mathrm{local},\mathbf{u}}$ into $\mathbf{K}_{\mathrm{nonlocal},\mathbf{u}}$.

By replacing (42) in (26), the consistent tangent matrix can be expressed as

$$\mathbf{K}_{\mathrm{tan}} = \mathbf{K}_{\mathrm{sec}} + \mathbf{K}_{\mathrm{local}} \mathbf{A} \,. \tag{44}$$

This simple structure of $\mathbf{K}_{\mathrm{tan}}$ is due to the fact that the nonlocal average is performed completely "upstream" in the constitutive equation (i.e. with displacements, the primal unknowns in the FE analysis).

4.2 Reliability

Even for nonlinear problems, simply *obtaining* a finite element solution is nowadays not enough. One must also ensure the quality of the numerical results in an objective, quantifiable manner. With that purpose, we present here an adaptive strategy based on error estimation [7,6]. The two key ingredients are a residual-type error estimator for nonlinear problems [24] and h-remeshing [25].

The issue of reliability is relevant in all fields of computational mechanics. In failure modelling of quasi-brittle materials, it is critical. Due to brittleness, the particular choice of a constitutive equation or a set of material parameters can have a very significant influence (not only quantitative but even qualitative) on the failure mechanism.

Of course, the finite element mesh also affects the numerical solution. For this reason, it is essential to keep FE errors under control when assessing the effect of material modelling. If models or sets of parameters are compared with a given mesh (deemed "sufficiently fine" but with no objective measure of its quality), the effect of FE discretization errors could be erroneously attributed to the different material models.

The key ingredient of the adaptive strategy is the error estimator. We use a residual-type error estimator first developed for linear problems in continua [26] and later extended to other problems, such as local nonlinear models, e.g. plasticity or visco-plasticity [24,27], nonlocal nonlinear models (nonlocal damage [6]), or (linear and nonlinear) shells [28].

The focus here is in the two main issues of the problem under consideration: nonlinearity and nonlocality. More details about the error estimator can be found in the references just cited.

4.2.1 Error Estimation: Nonlinearity

Finite element discretization of the governing partial differential equation renders the algebraic nonlinear equilibrium equation

$$\mathbf{f}_H^{\text{int}}(\mathbf{u}_H) = \mathbf{f}_H^{\text{ext}} \,, \tag{45}$$

where the unknown is the nodal displacement vector $\mathbf{u}_H$, $\mathbf{f}_H^{\text{int}}(\mathbf{u}_H)$ is the vector of nodal internal forces associated with $\mathbf{u}_H$ and $\mathbf{f}_H^{\text{ext}}$ is the discretized external force term. Subscript H denotes that the working mesh has characteristic size H.

The exact error of $\mathbf{u}_H$ is defined as $\mathbf{e}_{\mathbf{u}}^{\text{exact}} := \mathbf{u} - \mathbf{u}_H$, where $\mathbf{u}$ is the exact solution. Of course, $\mathbf{e}_{\mathbf{u}}^{\text{exact}}$ cannot be computed because $\mathbf{u}$ is not available. Instead, the error $\mathbf{e}_{\mathbf{u}}^{\text{exact}}$ is approximated by the reference error $\mathbf{e}_{\mathbf{u}} := \mathbf{u}_h - \mathbf{u}_H$, where $\mathbf{u}_h$ is the finite element solution obtained with a finer mesh ($h \ll H$, the approach considered here) or a higher-order interpolation:

$$\mathbf{f}_h^{\text{int}}(\mathbf{u}_h) = \mathbf{f}_h^{\text{ext}} \,. \tag{46}$$

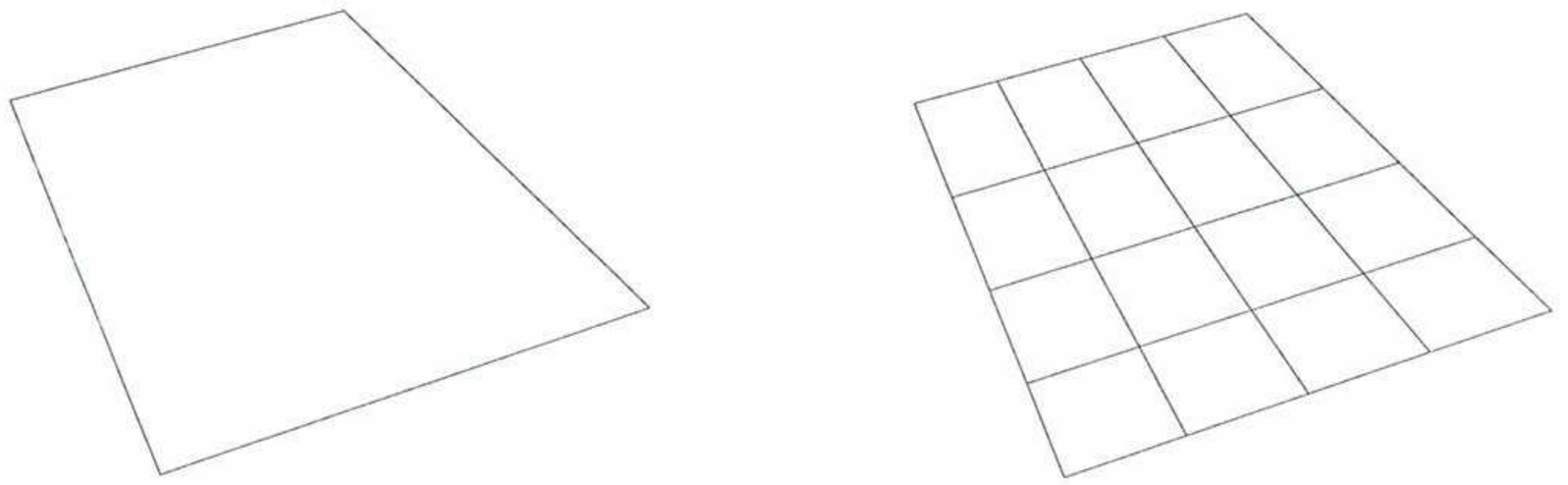

Figure 2. Finite element of mesh H subdivided into 4×4 elements of mesh h

Note that (46) can also be expressed as

$$\mathbf{f}_h^{\text{int}}(\mathbf{u}_H + \mathbf{e}_\mathbf{u}) = \mathbf{f}_h^{\text{ext}} \,. \tag{47}$$

Computing $\mathbf{e}_\mathbf{u}$ (or, equivalently, $\mathbf{u}_h$) is computationally much more expensive than computing $\mathbf{u}_H$, because it involves solving a much larger nonlinear system of equations over a finer mesh, (46) or (47). For this reason, the basic idea of residual-type error estimators is to approximate $\mathbf{e}_\mathbf{u}$ by low-cost local computations over subdomains.

The natural subdomains for local computations are the finite elements. For this reason, the first phase of the error estimator consists on solving the nonlinear system (47) locally inside each finite element of the working mesh (interior estimate, see Table 4). To do so, each element Ω_k of size H is meshed into 4×4 elements of size h, see Fig. 2. That it, the fine mesh h is nested into the working mesh H, with $H < h/4$.

To avoid the expensive flux-splitting procedures of other residual-type error estimators (required to prescribe Neumann boundary conditions for each local problem), homogeneous Dirichlet boundary conditions for the error are prescribed on the element boundary $\partial\Omega_k$ (that is, $\mathbf{u}_h = \mathbf{u}_H$ on $\partial\Omega_k$). This equality is also set, over all the element Ω_k, as the initial approximation. Once error $\mathbf{e}_{\text{elem}}^k$ is obtained, its squared energy norm (based on the SPD secant stiffness matrix) is computed and added up into the global error estimate.

Of course, the error $\mathbf{e}_\mathbf{u}$ is not really zero along all element edges, as assumed during the interior estimate. For this reason, a second set of local problems is solved, over a different partition of the computational domain into subdomains. A natural choice is to associate these subdomains, called patches, to the nodes of the working mesh (patch estimate, see Table 5). If four-noded quadrilateral elements are used, a patch consists of one-fourth of each element sharing the node, see Fig. 3.

To compute the estimate $\mathbf{e}_{\text{patch}}^\ell$ for patch Λ_ℓ, the same ideas discussed for

Table 4
Pseudocode for the first phase of the error estimation procedure. The interior estimate E is stored both locally ($\mathrm{E}(\Omega_k)$ for $k = 1, 2, \ldots$) and globally ($\mathrm{E}(\Omega)$ for the whole domain Ω)

loop on elements $k = 1, 2 \ldots$

- Build up local refined mesh for element Ω_k
- Set trivial Dirichlet b.c. $\mathbf{e}^k_{\mathrm{elem}} = \mathbf{0}$ on $\partial\Omega_k$
- Set initial approximation $\mathbf{e}^k_{\mathrm{elem}} = \mathbf{0}$ in Ω_k
- Solve iteratively local nonlinear problem

  $$\mathbf{r}(\mathbf{e}^k_{\mathrm{elem}}) := \mathbf{f}^{\mathrm{int}}_h(\mathbf{u}_H + \mathbf{e}^k_{\mathrm{elem}})|_{\Omega_k} - \mathbf{f}^{\mathrm{ext}}_h|_{\Omega_k} = \mathbf{0}$$

- Compute squared local norm

  $$\mathrm{E}(\Omega_k) = (\mathbf{e}^k_{\mathrm{elem}})^T \mathbf{K}^k_{\mathrm{sec},h} \mathbf{e}^k_{\mathrm{elem}}$$

- Store error function: $\mathbf{e}_{\mathrm{elem}} \leftarrow \mathbf{e}_{\mathrm{elem}} + \mathbf{e}^k_{\mathrm{elem}}$
- Upgrade global estimate: $\mathrm{E}(\Omega) \leftarrow \mathrm{E}(\Omega) + \mathrm{E}(\Omega_k)$

end loop

Interior estimate

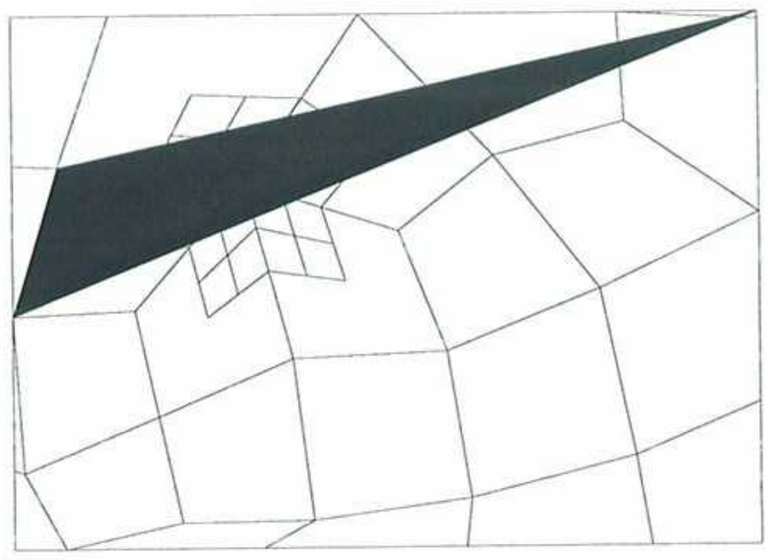

Figure 3. Patch associated to a node of mesh H subdivided into 4×4 elements of mesh h

elements apply. Again, the boundary conditions and the initial approximation for the local nonlinear problem over the patch consist in setting $\boldsymbol{\eta}^\ell$ to zero over $\partial\Lambda_\ell$ and Λ_ℓ respectively.

The only difference is that orthogonality between patch estimate $\boldsymbol{\eta}^\ell$ and interior estimate $\boldsymbol{\varepsilon}$ must be imposed, to avoid accounting for the same error contribution twice. If the Lagrange multiplier is used for boundary conditions, then the orthogonality restriction can be prescribed as an additional "bound-

Table 5
Pseudocode for the second phase of the error estimation procedure. The patch estimate is used to improve the estimate both locally ($\mathrm{E}(\Omega_k)$ for $k = 1, 2, \ldots$) and globally ($\mathrm{E}(\Omega)$ for the whole domain Ω)

loop on patches $\ell = 1, 2 \ldots$

- Build up local refined mesh for patch Λ_ℓ
- Set trivial Dirichlet b.c. $\mathbf{e}^\ell_{\text{patch}} = \mathbf{0}$ on $\partial\Lambda_\ell$

  + orthogonality to $\mathbf{e}_{\text{elem}}$
- Set initial approximation $\mathbf{e}^\ell_{\text{patch}} = \mathbf{0}$ in Λ_ℓ
- Solve iteratively local nonlinear problem

  $\mathbf{r}(\mathbf{e}^\ell_{\text{patch}}) := \mathbf{f}^{\text{int}}_h(\mathbf{u}_H + \mathbf{e}^\ell_{\text{patch}})|_{\Lambda_\ell} - \mathbf{f}^{\text{ext}}_h|_{\Lambda_\ell} = \mathbf{0}$
- Compute squared local norm

  $\mathrm{E}(\Lambda^\ell) = (\mathbf{e}^\ell_{\text{patch}})^T \mathbf{K}^\ell_{\text{sec},h} \mathbf{e}^\ell_{\text{patch}}$
- Upgrade global estimate: $\mathrm{E}(\Omega) \leftarrow \mathrm{E}(\Omega) + \mathrm{E}(\Lambda_\ell)$
- Upgrade local (element) estimate:

  $n^\ell_{\text{over}} =$ number of elements overlapping Λ_ℓ

  for k such that $\Omega_k \cap \Lambda_\ell \neq \emptyset$

  $\mathrm{E}(\Omega_k) \leftarrow \mathrm{E}(\Omega_k) + \mathrm{E}(\Lambda_\ell)/n^\ell_{\text{over}}$

end loop

Patch estimate

ary" condition is a simple manner [24].

The proposed two-phase approach for error estimation is summarized in Tables 4 and 5.

4.2.2 Error Estimation: Nonlocality

The proposed two-phase approach for error estimation consists basically in solving two sequences of *local* nonlinear problems over subdomains (elements and patches), see Tables 4 and 5. The material model, however, is nonlocal. As a consequence, the internal forces $\mathbf{f}_{\text{int}}$ must be carefully computed in order to account for the nonlocal nature of the damage model [6].

The "natural" approach would be, see central column of Table 6, to obtain the

Table 6
Standard nonlocal damage model and model modified for error estimation. Note the difference in the computation of the nonlocal state variable, steps 4 and 5

	Standard model	**Model for error estimation**
1. Error in displ.	$\mathbf{e_u}$	$\mathbf{e_u}$
2. Error in strains	$\mathbf{e}_\varepsilon = \nabla^s(\mathbf{e_u})$	$\mathbf{e}_\varepsilon = \nabla^s(\mathbf{e_u})$
3. Strain	$\varepsilon_h = \varepsilon_H + \mathbf{e}_\varepsilon$	$\varepsilon_h = \varepsilon_H + \mathbf{e}_\varepsilon$
4. Local state var.	$Y_h = Y(\varepsilon_h)$	$Y_h \approx Y_H + \underbrace{\frac{\partial Y}{\partial \varepsilon}(\varepsilon_H)\mathbf{e}_\varepsilon}_{e_Y\text{: Error in } Y}$
5. Nonlocal state var.	$\widetilde{Y}_h = \mathrm{NLA}_{\mathrm{sub}}(Y_h)$	$e_{\widetilde{Y}} = \mathrm{NLA}_{\mathrm{sub}}(e_Y)$; $\widetilde{Y}_h = \widetilde{Y}_H + e_{\widetilde{Y}}$
6. Damage	$D_h = D(\widetilde{Y}_h)$	$D_h = D(\widetilde{Y}_h)$
7. Stresses	$\boldsymbol{\sigma}_h = (1 - D_h)\mathbf{C} : \varepsilon_h$	$\boldsymbol{\sigma}_h = (1 - D_h)\mathbf{C} : \varepsilon_h$

error in strains $\mathbf{e}_\varepsilon$ from the error in displacements $\mathbf{e_u}$ (in the corresponding element or patch), compute the refined strains ε_h and the local state variable Y_h. The nonlocal average over the subdomain (element k or patch ℓ), $\mathrm{NLA}_{\mathrm{sub}}$, then yields the nonlocal state variable $\widetilde{Y}_h$, which drives the damage parameter, D_h. Finally, refined stresses $\boldsymbol{\sigma}_h$ are computed.

Note that the nonlocal average that transforms Y_h into $\widetilde{Y}_h$ is over a local support. This fact leads to non-physical responses, especially in zones of large damage gradients. Assume, for instance, that the error in strains is small and $\varepsilon_h \approx \varepsilon_H$. A small variation in $\widetilde{Y}$ is also expected ($\widetilde{Y}_h \approx \widetilde{Y}_H$). However, it may happen that $\widetilde{Y}_h \ll \widetilde{Y}_H$, because $\widetilde{Y}_h$ contains no information about nearby zones.

This point is illustrated in Fig. 4, which depicts the local state variable, the nonlocal state variable and the damage parameter for a given time increment in a zone of the working mesh H with large gradients. The circled element has a very small local state variable Y_H, see Fig. 4(a), below the threshold Y_0. However, since the elements to the right have large values of Y_H, it has a relatively large (above Y_0) nonlocal state variable $\widetilde{Y}_H$, see Fig. 4(b), which leads to damage, see Fig. 4(c). If the standard model is used to solve the local problem on the circled element during error estimation, a small error in strains leads to a small variation in the local state variable which, after nonlocal averaging over the element, results in a low value of the nonlocal state variable (that is, $\widetilde{Y}_h \ll \widetilde{Y}_H$). As a consequence, damage cannot increase

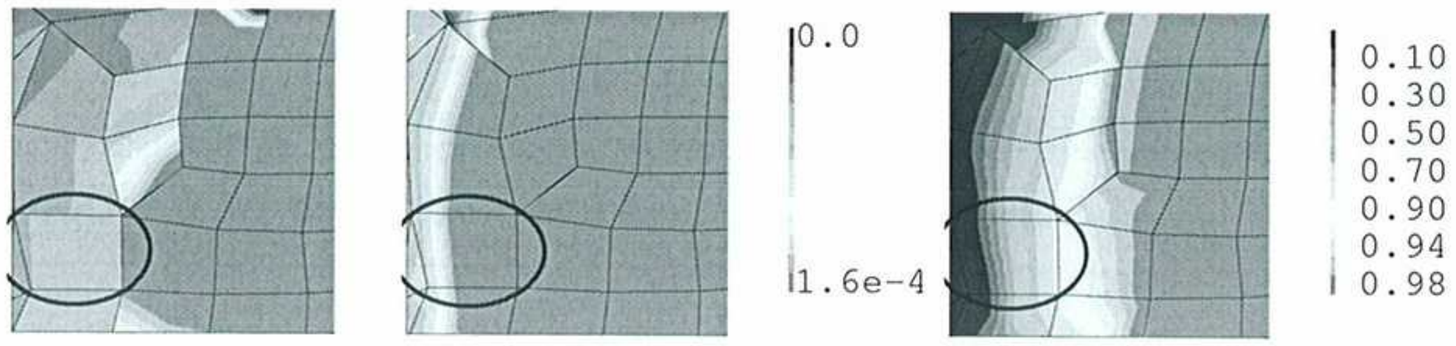

(a) (b) (c)

Figure 4. Fields in a zone of large gradients: (**a**) local state variable Y; (**b**) nonlocal state variable $\widetilde{Y}$; (**c**) damage. The damage threshold is $Y_0 = 1.5 \times 10^{-4}$

in the circled element during error estimation. When estimating the error for the circled element, the nonlocal state variable $\widetilde{Y}_H$, rather than the local state variable Y_H, is representative of its mechanical properties.

For this reason, the nonlocal damage model is slightly modified for error estimation, see right column in Table 6. The difference resides in the way the nonlocal state variable $\widetilde{Y}_h$ is computed. By means of a first-order Taylor expansion, the local state variable Y_h is expressed as Y_H plus an error term e_Y. Note that the derivatives $\partial Y/\partial \boldsymbol{\varepsilon}$ needed for computing e_Y are also required for the computation of the consistent tangent matrix, so they do not represent a computational overhead of the modified model.

The error term e_Y is averaged over the element/patch into $e_{\widetilde{Y}}$. As a consequence, $\widetilde{Y}_h$ is computed as the addition of a reference value $\widetilde{Y}_H$, which describes the real damaged stiffness, and an error term $e_{\widetilde{Y}}$.

With this modified model, a small variation in strains does result in a small variation in the nonlocal state variable (that is, $\widetilde{Y}_h \approx \widetilde{Y}_H$). Going back to figure 4, this means that the damage level of the circled element may either remain constant (for $\widetilde{Y}_h < \widetilde{Y}_H$) or increase (for $\widetilde{Y}_h > \widetilde{Y}_H$) during error estimation.

To sum up: the standard model is not capable of capturing the spread of the damaged zone associated to error estimation.

5 Applications

In this section, various representative numerical examples are described in detail. First, the behaviour of the proposed model based on nonlocal displacements is illustrated by means of a simple uniaxial test. After that, three experimental tests (the three-point bending test, the single-edge notched beam test, and the Brazilian cylinder-splitting test) are modelled with standard nonlocal damage models. The goal is to discuss, among others, the following issues: the performance of the proposed adaptive strategy based on error estimation; the

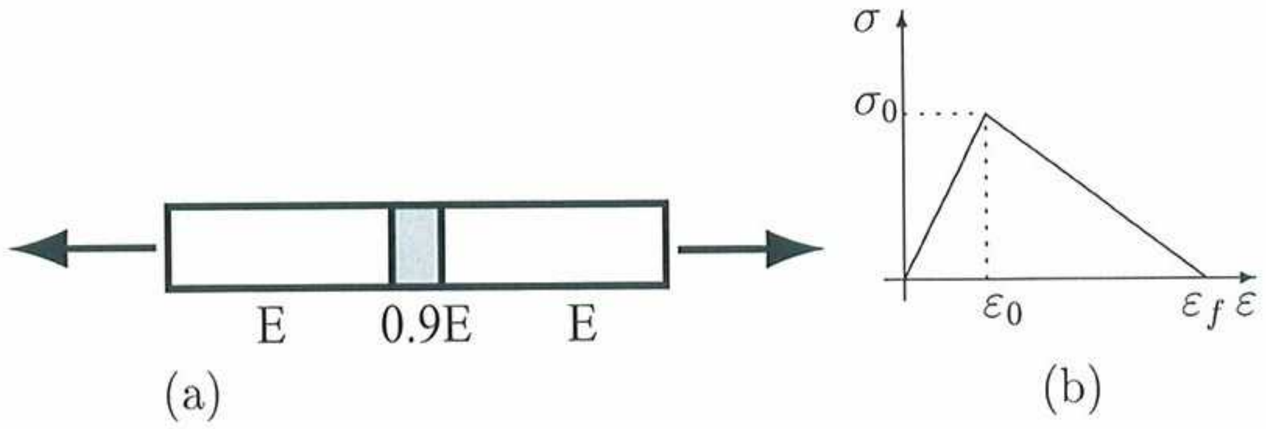

Figure 5. Uniaxial tension test: (**a**) problem statement; (**b**) linear softening law

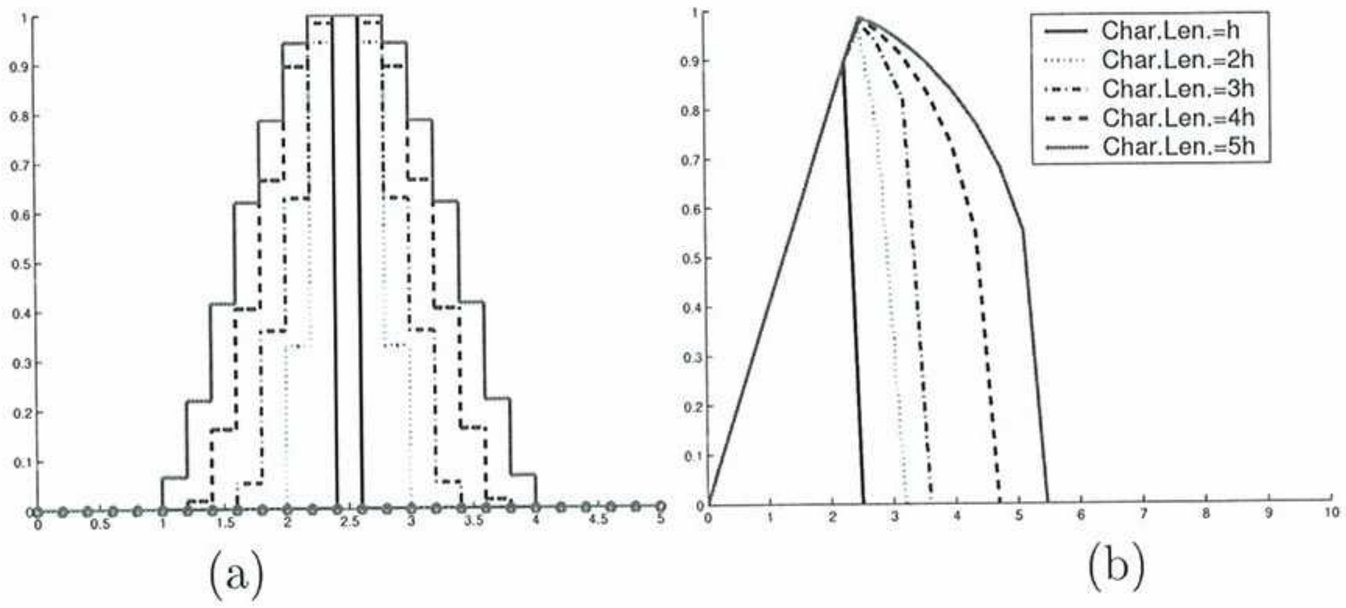

Figure 6. Uniaxial tension test with various characteristic lengths. (**a**) final damage profiles; (**b**) force-displacement curves

influence of the material parameters on the structural response; the ability of the proposed approach to capture complex failure mechanisms; the comparative performance of the various stiffness matrices; the effect of exploiting problem symmetry on the failure pattern.

5.1 Uniaxial Tension Test

A bar is subjected to uniaxial tension, see Fig. 5(a). The one-dimensional version of the damage model based on nonlocal displacements, see Table 2, with $Y(\varepsilon) = \varepsilon$ and a linear softening law, see Fig. 5(b), is used. The central finite element is weakened (10% reduction in Young's modulus) to trigger localization.

The qualitative behaviour of the model is illustrated in Fig. 6. A fixed mesh of 25 elements and five different characteristic lengths (from $l_c = h$ to $l_c = 5h$) have been used. Figs. 6(a) and 6(b) show respectively the final damage profile and the force-displacement curve. Note that, as desired, the width of the damage zone and the brittleness of the structural response is controlled by the characteristic length.

To check the regularization capability of the model, the test is reproduced with four different meshes (of 15, 25, 35 and 45 finite elements) and three

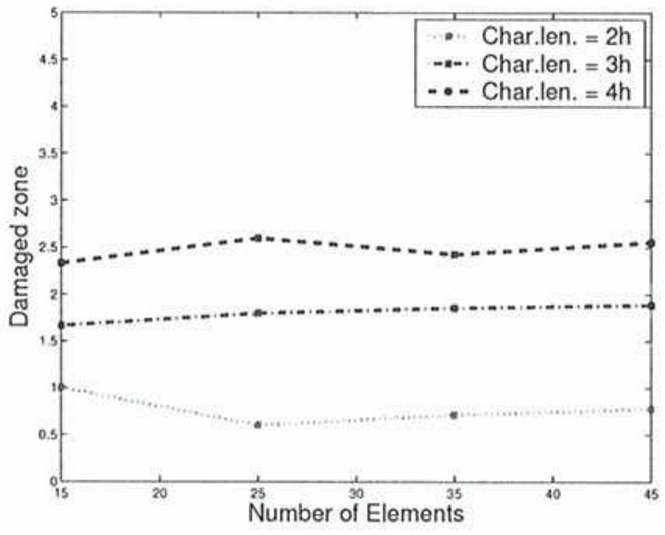

Figure 7. Uniaxial tension test. Width of damage profile for different meshes and characteristic lengths

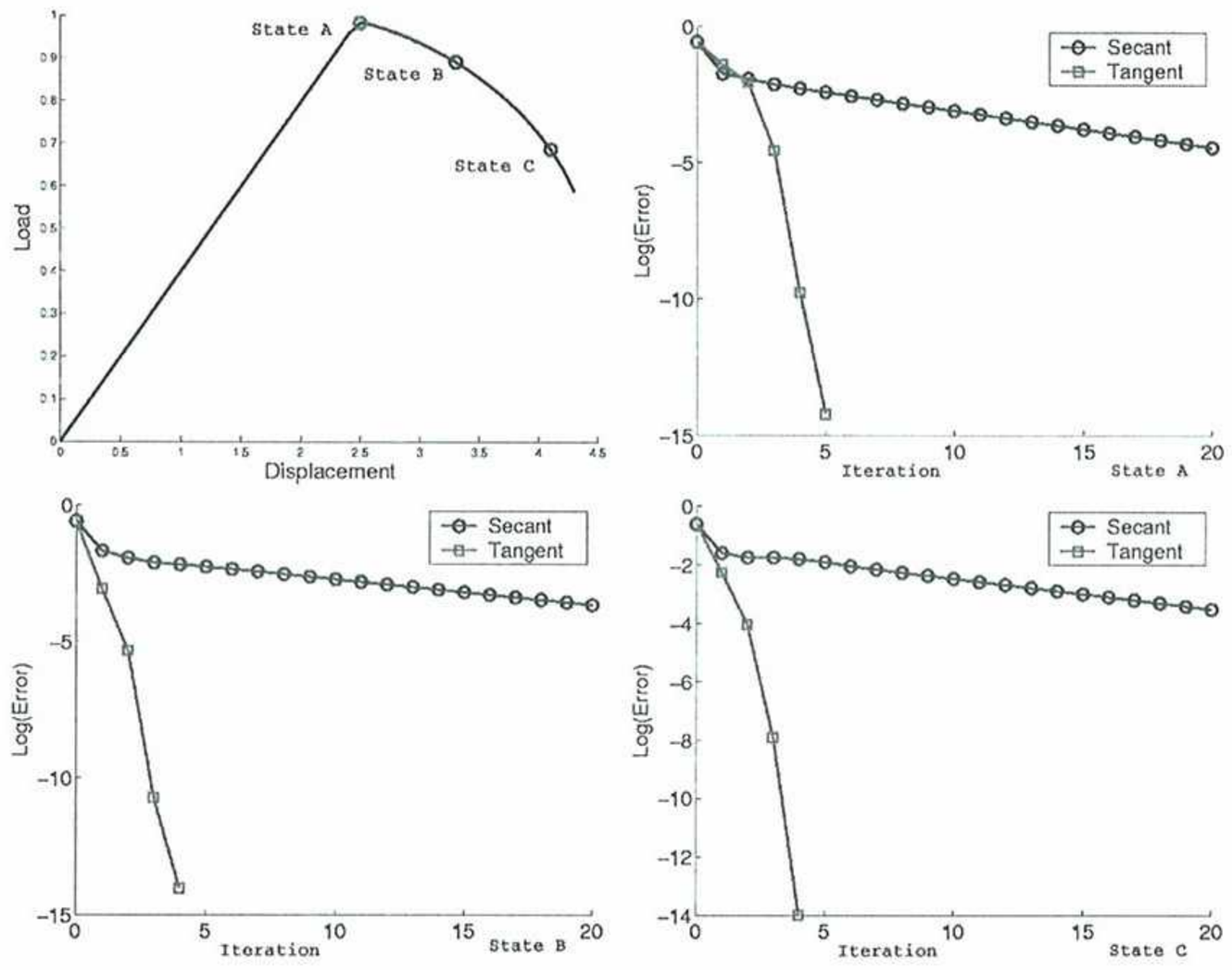

Figure 8. Uniaxial tension test. Convergence history of the secant matrix and the consistent tangent matrix

different characteristic lengths. Figure 7 shows clearly that the width of the final damage profile is controlled by the characteristic length, and not by the element size. Mesh dependence is indeed precluded with this damage model.

Figure 8 shows the convergence behaviour with two different nonlinear solvers at representative load steps and iterations. As expected, only linear convergence is achieved with the secant stiffness matrix, while the consistent tangent matrix derived in Sect. 4.1.4 leads to quadratic convergence.

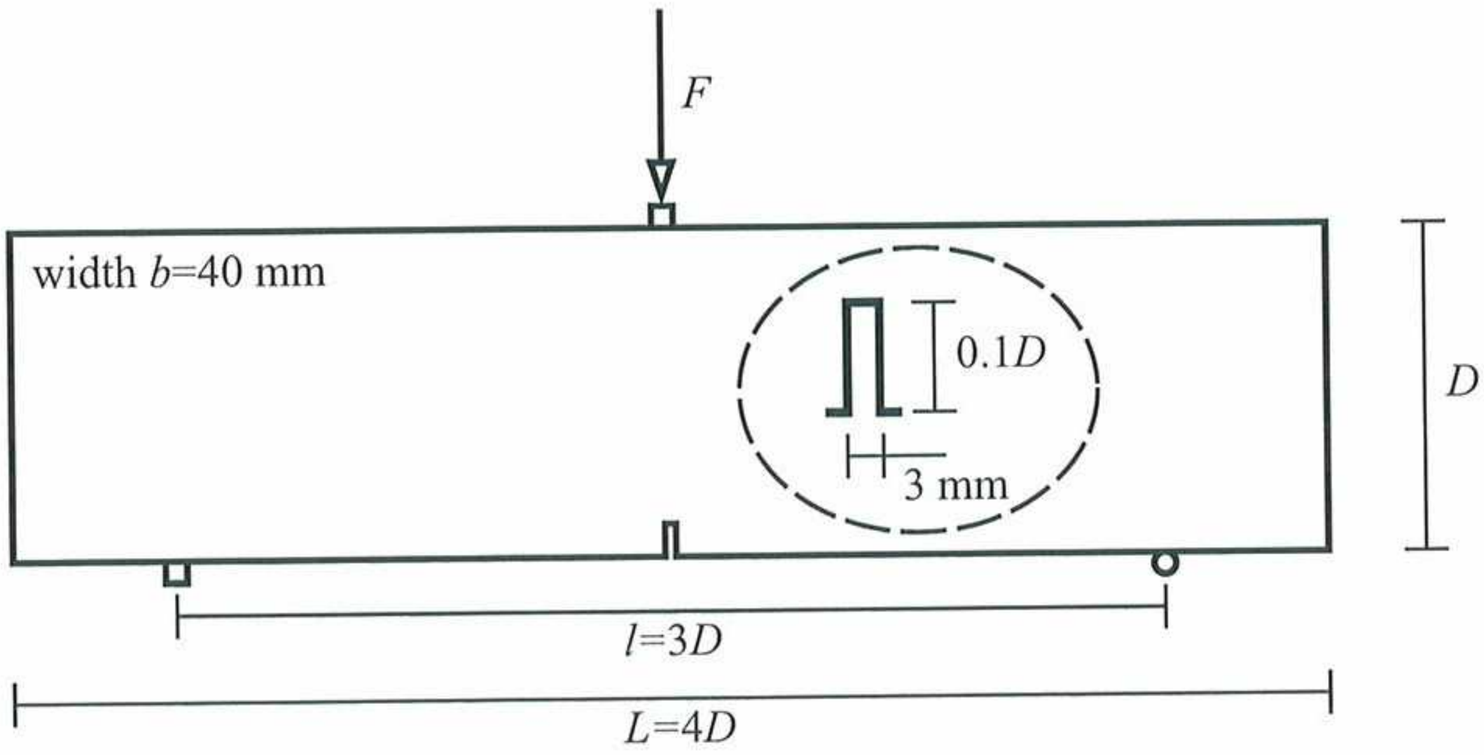

Figure 9. Three-point bending test. Problem statement (Size D=320 mm)

Table 7
Three-point bending test. Material parameters for the Mazars model [29]

Meaning	**Symbol**	**Value**
Young's modulus	E	38 500 MPa
Poisson's coefficient	ν	0.24
Characteristic length	l_c	40 mm
Damage threshold	Y_0	3×10^{-5}
Parameter A in compression	A_c	1.25
Parameter B in compression	B_c	1000
Parameter A in tension	A_t	0.95
Parameter B in tension	B_t	9000

5.2 Three-Point Bending Test

A notched beam is subjected to three-point bending, see Fig. 9. This test is modelled with the Mazars model [12] and the material parameters obtained in [29], see Table 7, by fitting the results of various experiments. Plane strain conditions are assumed.

If a displacement control strategy (with vertical deflection of the point under the load as the control variable) is used, the structural response of Fig. 10 is obtained. Note the abrupt softening behaviour after the peak load, typical of quasi-brittle materials.

Both in the force-deflection and the force-COD (crack-opening displacement) curves, Figs. 10(a) and 10(b), the softening branch exhibits, at its beginning

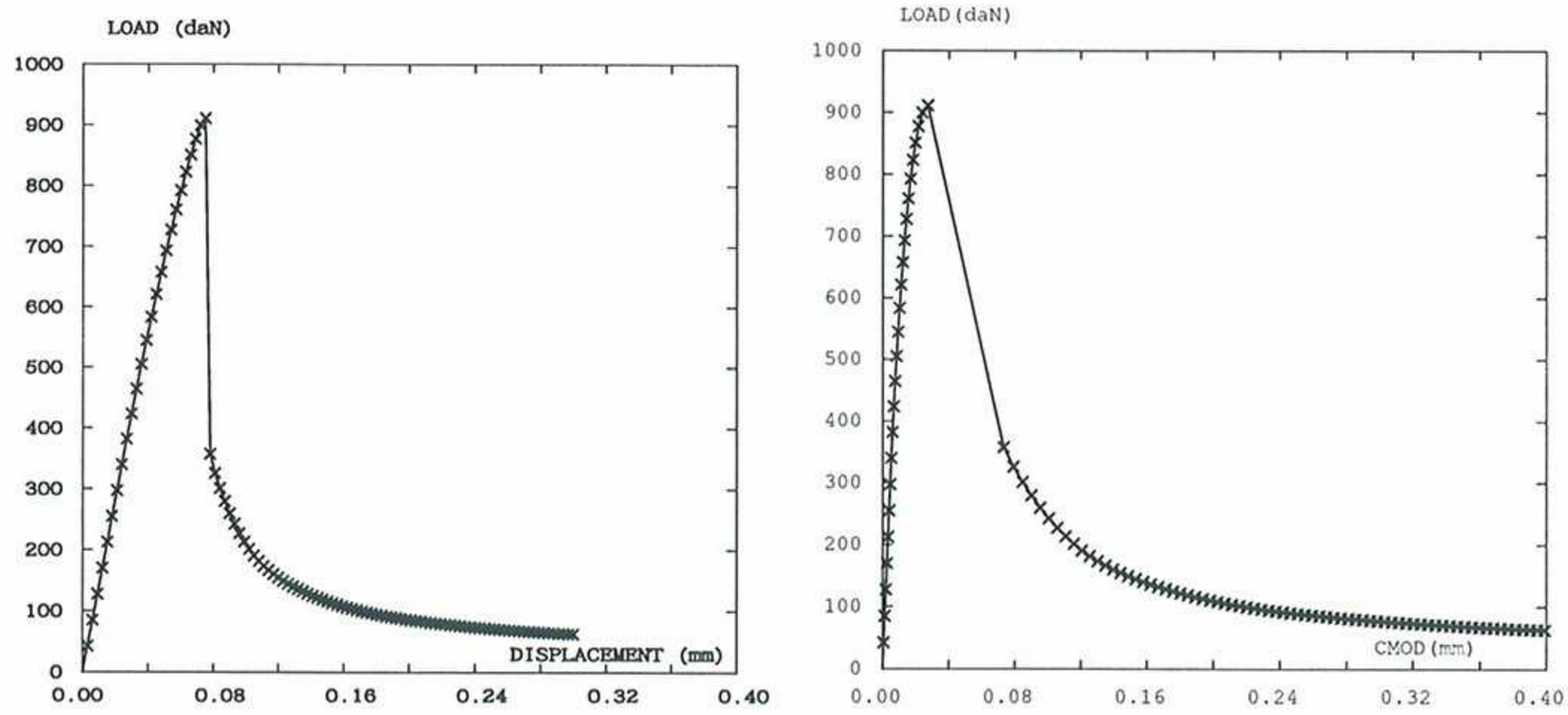

(a) (b)

Figure 10. Three-point bending test. Structural response obtained with displacement control: (**a**) force-vertical deflection; (**b**) force-COD (crack opening displacement)

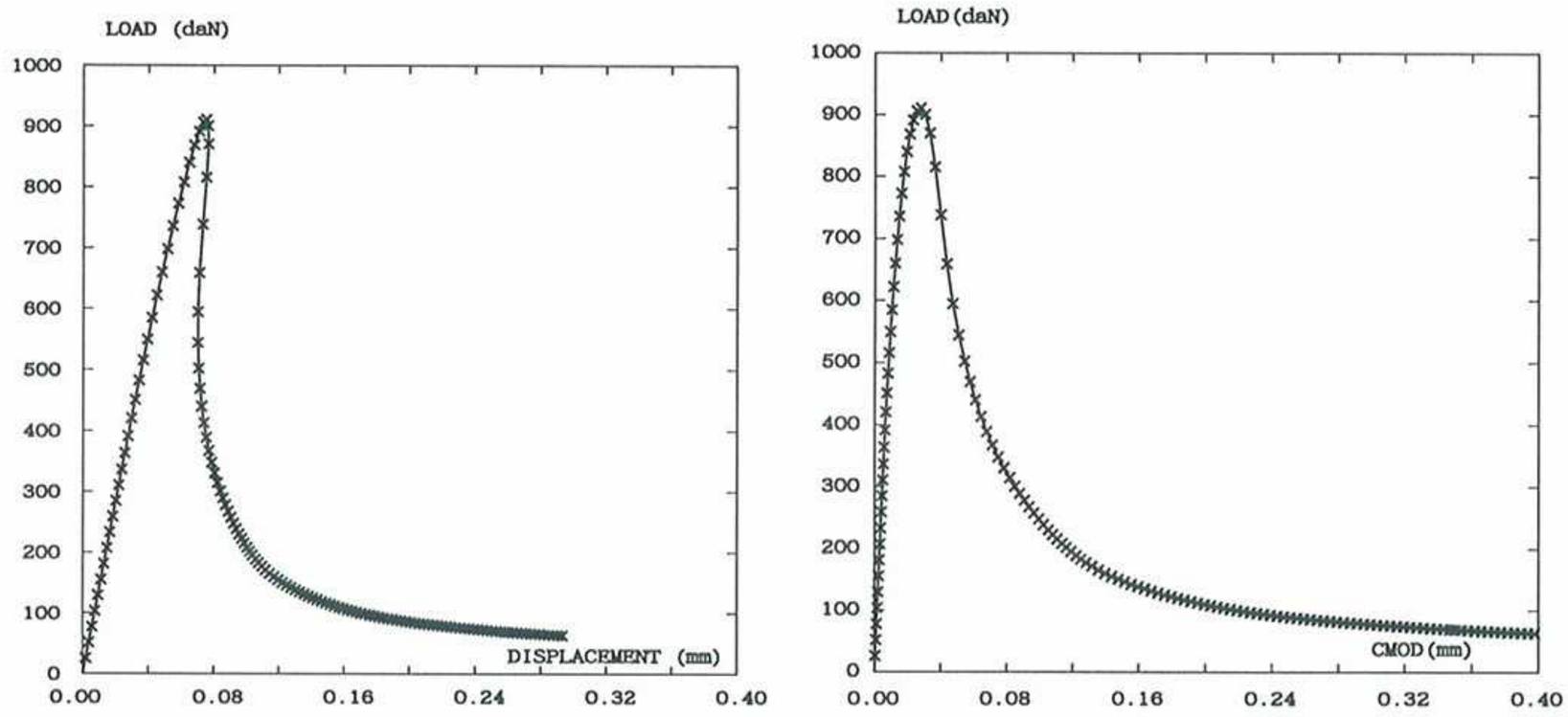

(a) (b)

Figure 11. Three-point bending test. Structural response obtained with arc-length control: (**a**) force-vertical deflection; (**b**) force-COD (crack opening displacement)

a "suspicious" straight segment. To check its meaning, the numerical test is repeated with a different control strategy: arc-length control with $\Delta s = |\Delta \mathrm{COD}|$. The results are depicted in Fig. 11.

Figure 11(a) clearly shows that the force-deflection curve exhibits a certain amount of snap-back behaviour, which cannot be captured with a displacement control strategy, Fig. 10, which assumes that the control variable (i.e. the deflection in this case) increases monotonically.

Since the snap-back is moderate, there is not much difference between Figs. 10 and 11. For other problems, however, the appropriate combination of control strategy and control variable is critical in tracking the nonlinear response [30].

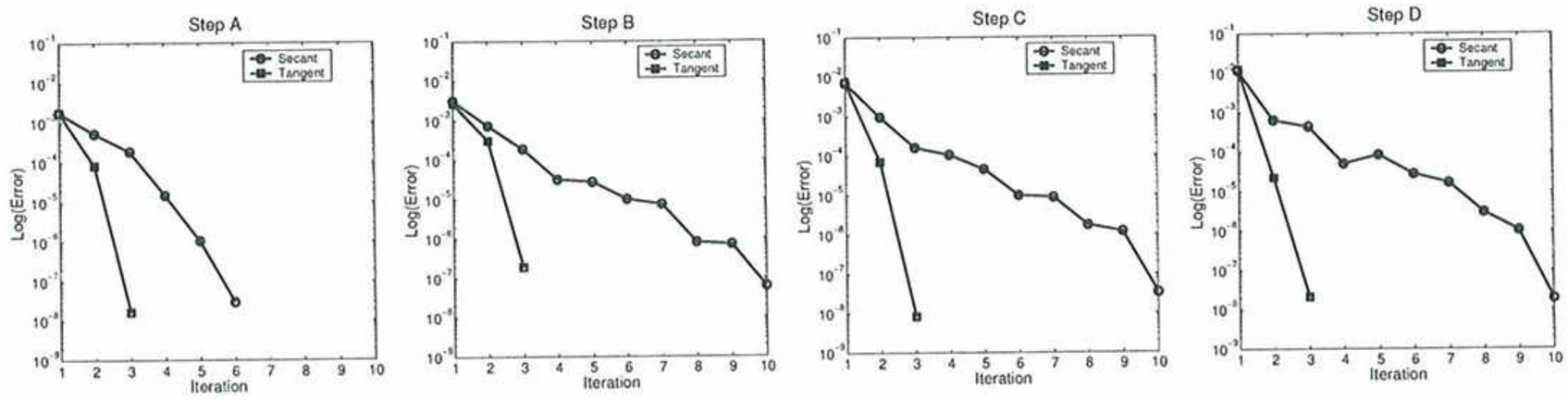

Figure 12. Three-point bending test. Convergence history for representative load-steps with the secant matrix and the consistent tangent matrix

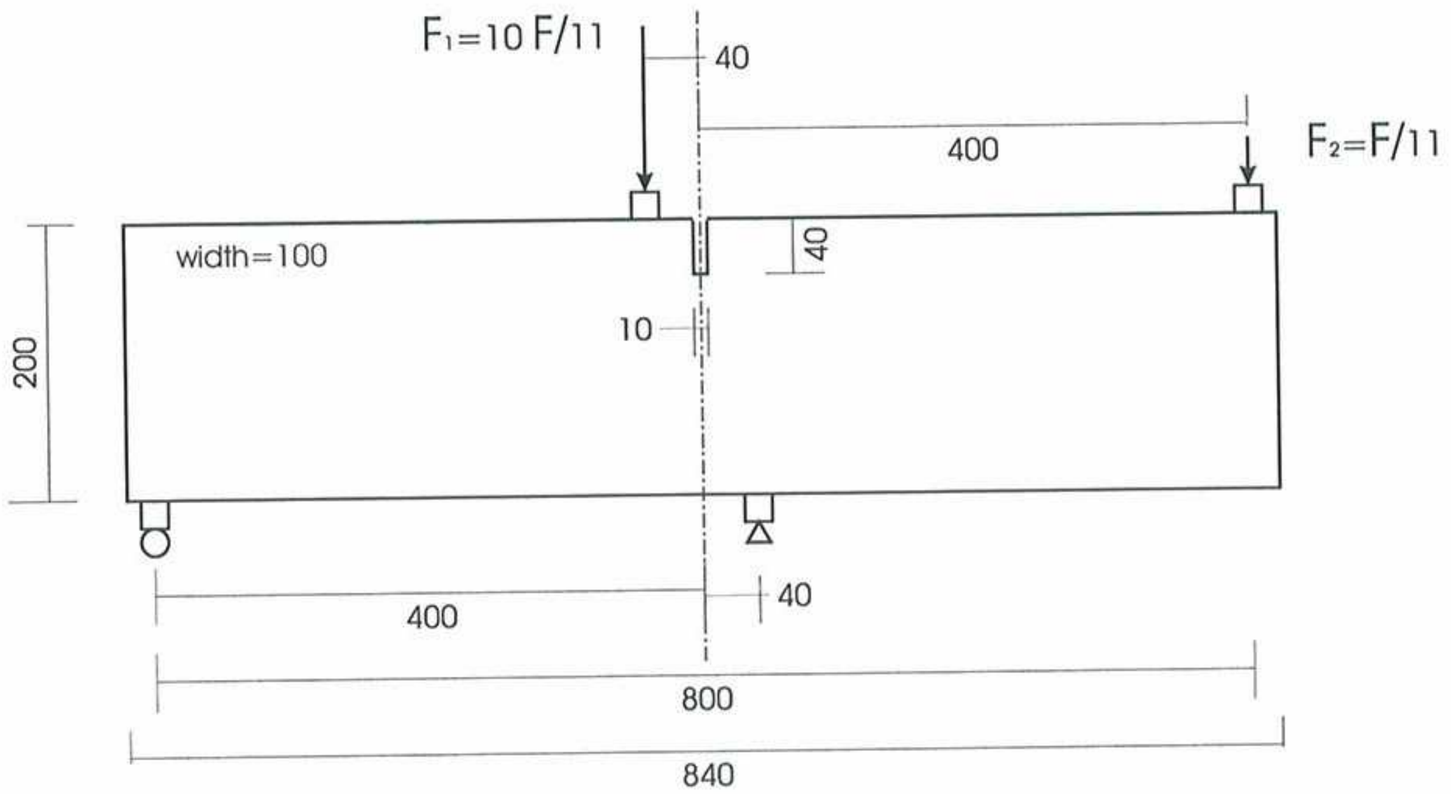

Figure 13. Single-edge notched beam. Problem statement (all distances in mm)

The convergence behaviour of the various nonlinear solvers is summarized is Fig. 12. Note that quadratic convergence is achieved with the consistent tangent matrix, while only linear convergence is obtained with the secant matrix.

5.3 Single-Edge Notched Beam Test

A single-edge notched beam (SENB) is subjected to anti-symmetrical four-point bending [31]. The geometry, loads and supports are shown in Fig. 13. A plane stress analysis is performed. The concrete beam is modelled with the modified von Mises nonlocal damage model [13] with exponential damage evolution, while the steel loading platens are assumed to be elastic.

Two sets of material parameters are used for concrete [6], see Table 8. For material 1, there is a significant post-peak softening in the stress-strain law for concrete. For material 2, on the contrary, the softening is very slight, so the residual strength almost coincides with the peak strength [32]. For steel, a

Table 8
SENB test. The two sets of material parameters: large softening (material 1) and very slight softening (material 2)

		Value	
Meaning	**Symbol**	**Material 1**	**Material 2**
Young's modulus	E	28 000 MPa	35 000 MPa
Poisson's coefficient	ν	0.1	0.2
Characteristic length	l_c	10 mm	10 mm
Damage threshold	Y_0	1.5×10^{-4}	6.0×10^{-5}
Parameter A	A	0.8	0.08
Parameter B	B	9 000	8 200

Poisson's coefficient $\nu = 0.2$ and a Young's modulus 10 times that of concrete are used.

5.3.1 SENB Test with Material 1

The results with material 1 are shown in Figs. 14–16. The initial mesh is shown in Fig. 14(a). Note that this mesh is relatively coarse, with only one element in the notch width. The final damage distribution and deformed mesh (amplified 300 times), corresponding to a CMSD of 0.08 mm, is depicted in Fig. 14(b). The curved crack pattern observed in experiments [31] is clearly captured. The error estimation procedure discussed in Sect. 4.2 is employed to compute the error field of Fig. 14(d). The error is larger in the damaged zone and near the loading platens. The global relative error (i.e. energy norm of the error in displacements over the energy norm of displacements) is 3.96%, above a threshold set a priori of 2%, so adaptivity is required.

The error field of Fig. 14(d) is translated into the mesh of Fig. 15(a). Note the element concentration in the crack and the central supports. This finer mesh leads to a better definition of the damaged zone, see Fig. 15(b). The error estimator now detects that the largest errors are associated to the *edges* of the cracked zone, see Fig. 15(d). The global relative error of 2.11% is still slightly above the error goal, so another adaptive iteration is performed. The outcome of this second iteration is shown in Fig. 16. The qualitative results of iteration 1 are confirmed: (1) small elements are needed to control the error in the damaged zones and close to the loading platens and (2) error is larger in the edges than in the centre of the crack. The global relative error of 1.77% is below the threshold of 2%, so the adaptive iterative process stops.

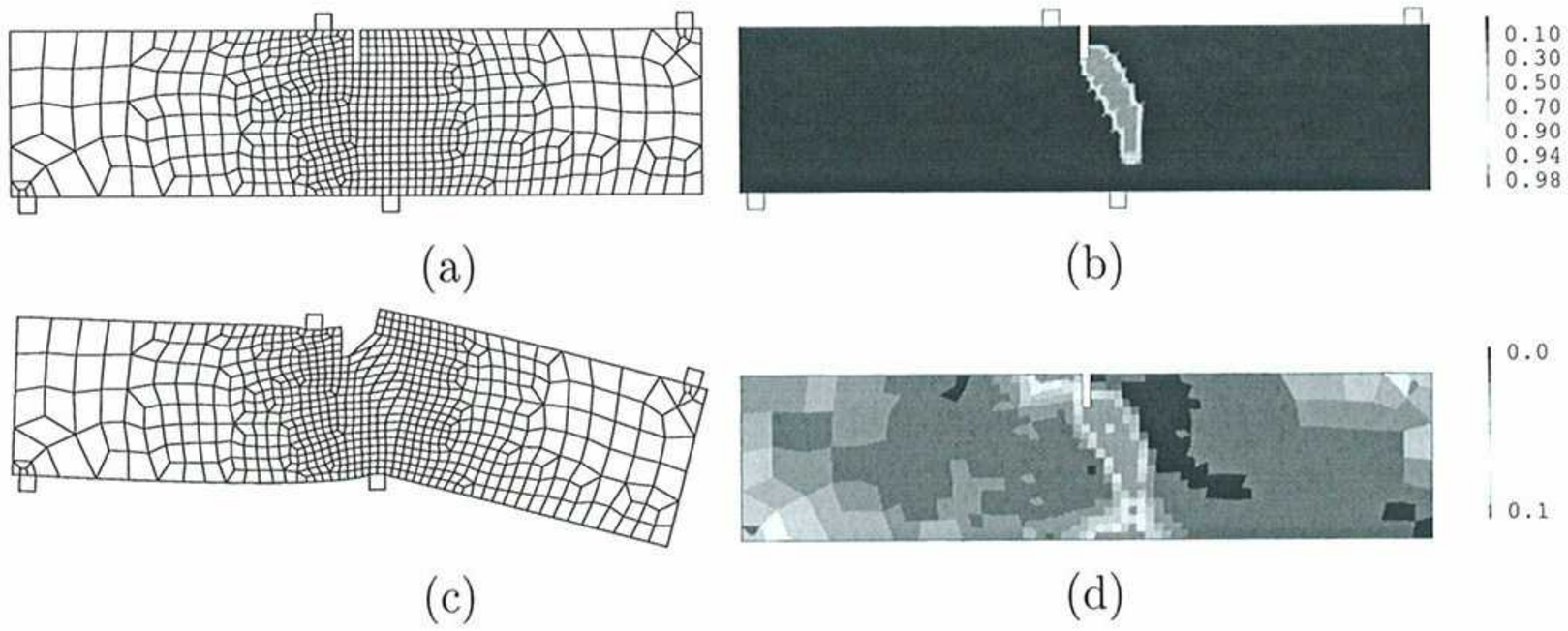

Figure 14. SENB test. Material 1, initial approx. (**a**) Mesh 0: 659 elem., 719 nodes; (**b**) damage; (**c**) deformed mesh (×300); (**d**) error field. Global relative error: 3.96%

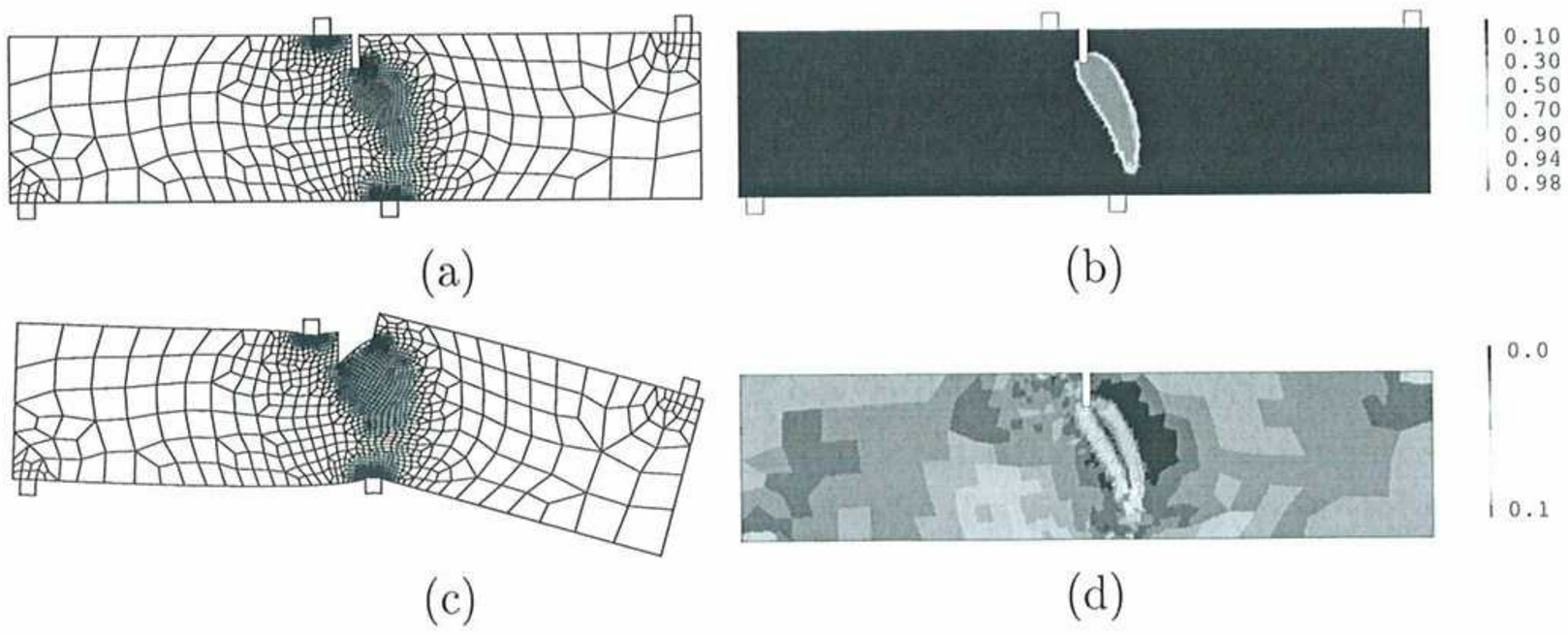

Figure 15. SENB test. Material 1, iteration 1. (**a**) Mesh 1: 1155 elem., 1228 nodes; (**b**) damage; (**c**) deformed mesh (×300); (**d**) error field. Global relative error: 2.11%

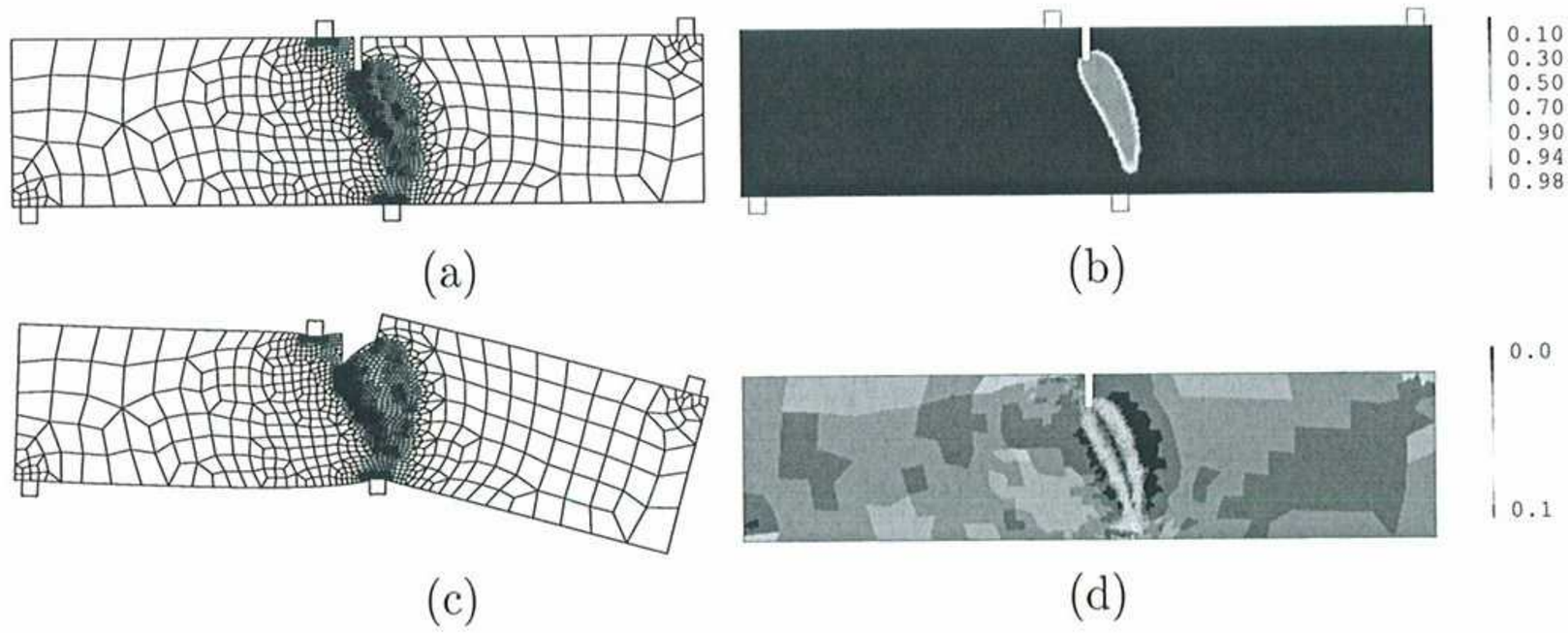

Figure 16. SENB test. Material 1, iteration 2. (**a**) Mesh 2: 1389 elem., 1469 nodes; (**b**) damage; (**c**) deformed mesh (×300); (**d**) error field. Global relative error: 1.77%

5.3.2 SENB Test with Material 2

The SENB test is now reproduced with material 2, which has a stress-strain law with almost no softening [6]. A very similar law has been employed to simulate the SENB test with gradient-enhanced damage models [32].

The results are shown in Figs. 17–19. The initial mesh is the same as before, see Fig. 17(a). The change in the material parameters leads to a completely different failure pattern, dominated by bending of opposite sign in the two halves of the beam, see Figs. 17(b) and 17(c). A crack at the notch tip is also initiated, but it is only a secondary mechanism. The error estimation procedure has no difficulties in reflecting the change in the failure mode, see Fig. 17(d). The global relative error is 3.66%, so adaptivity is required.

Figures 18 and 19 illustrate the adaptive process. Note that meshes 1 and 2 are quite different from the ones obtained with material 1. The global relative errors are 2.46% and 2.13%. This value is still slightly above the threshold of 2%. However, an additional iteration is considered not necessary for the illustrative purpose of this test.

A final comparison between the two sets of material parameters is offered by Fig. 20, where the total load is plotted versus the CMSD for meshes 0 and 2. The results obtained with material 1 – a peak load of around 60 kN (with mesh 2) and post-peak structural softening, see Fig. 20(a) – are in good agreement with the experiments [31]. With material 2, on the other hand, the peak load is quite higher and no softening is observed, see Fig. 20(b).

As a final remark, note that Fig. 20 also shows a significant quantitative difference between the solutions with meshes 0 and 2. The result with the initial mesh clearly overestimates the peak load. The adaptive strategy based on error estimation enables an accurate prediction of the structural response.

5.4 Brazilian Test

The Brazilian (or cylinder-splitting) test provides an indirect measure of tensile strength of quasi-brittle materials. A cylindrical specimen is loaded along a diametral plane, see Fig. 21.

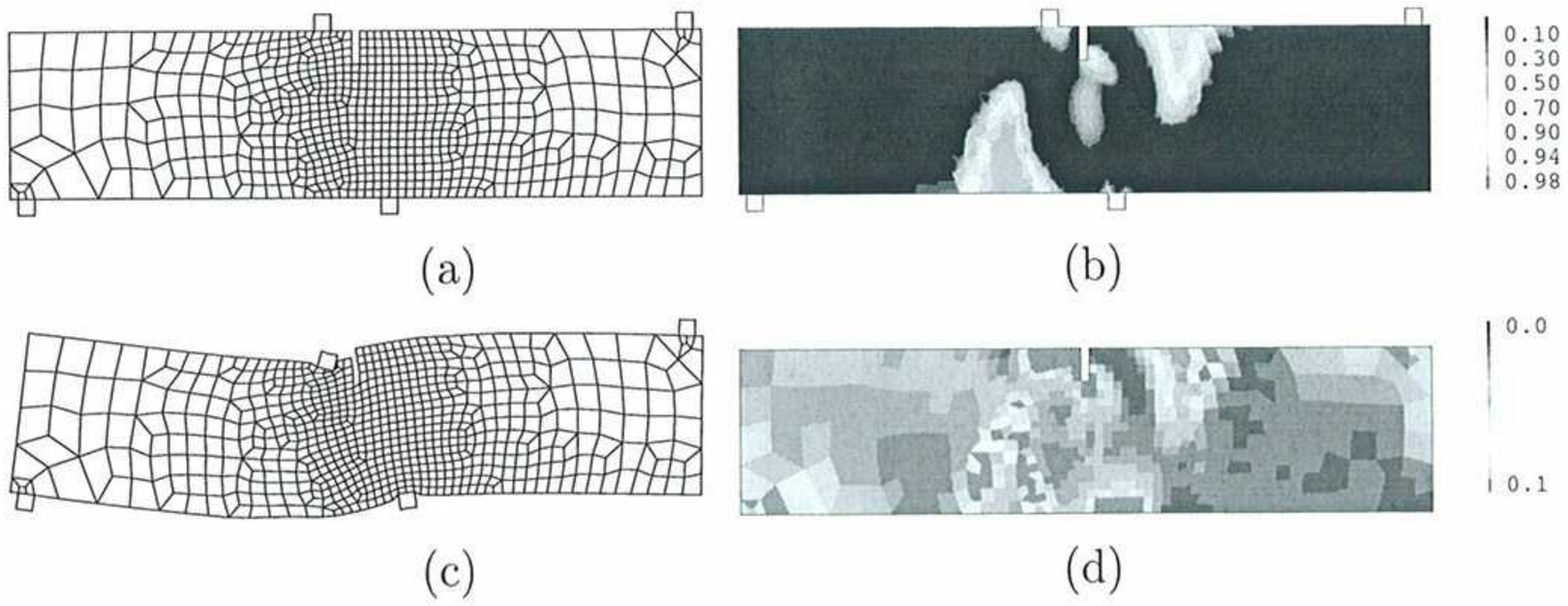

Figure 17. SENB test. Material 2, initial approx. (**a**) Mesh 0: 659 elem., 719 nodes; (**b**) damage; (**c**) deformed mesh (×300); (**d**) error field. Global relative error: 3.66%

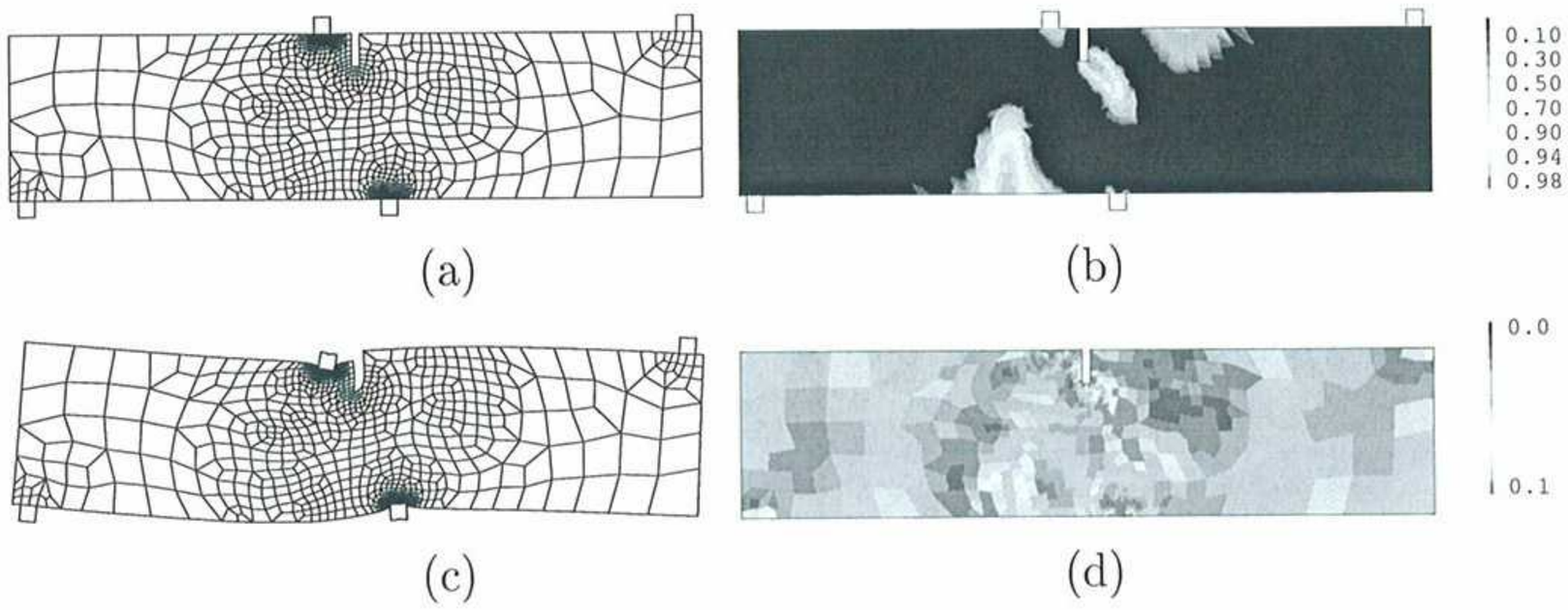

Figure 18. SENB test. Material 2, iteration 1. (**a**) Mesh 1: 776 elem., 848 nodes; (**b**) damage; (**c**) deformed mesh (×300); (**d**) error field. Global relative error: 2.46%

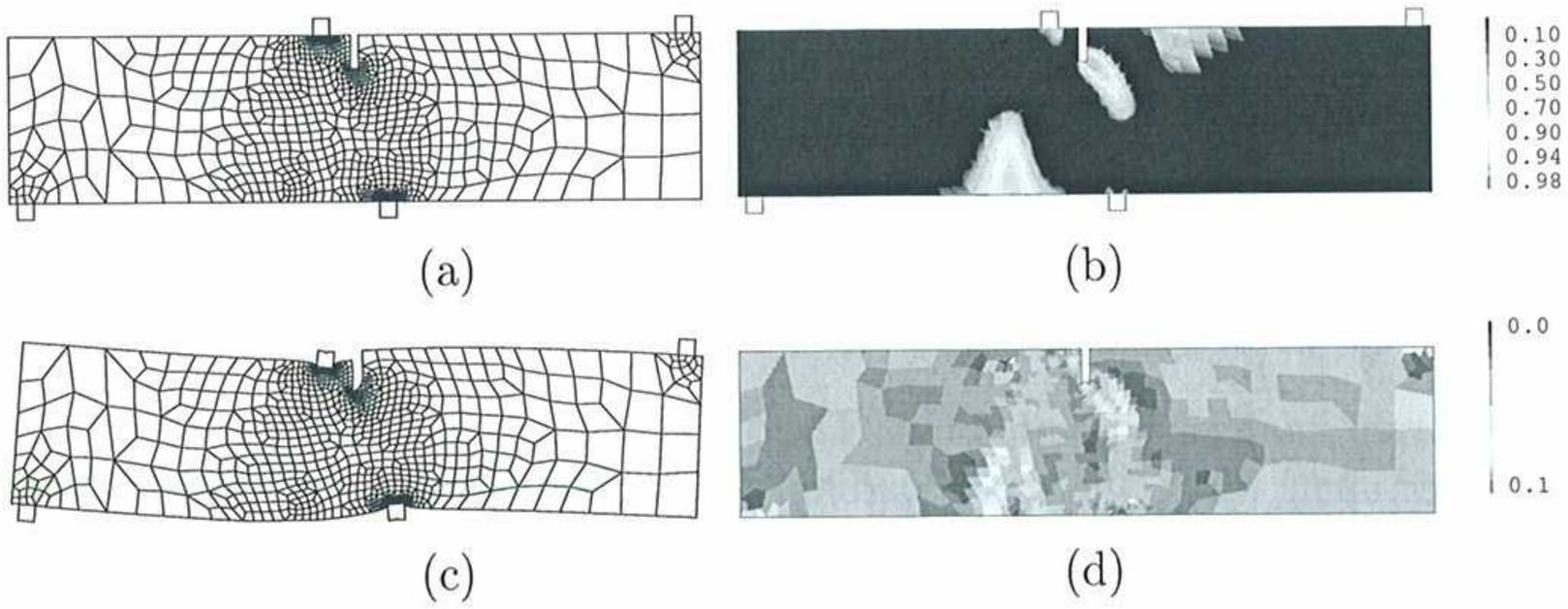

Figure 19. SENB test. Material 2, iteration 2. (**a**) Mesh 2: 870 elem., and 954 nodes; (**b**) damage; (**c**) deformed mesh (×300); (**d**) error field. Global relative error: 2.13%

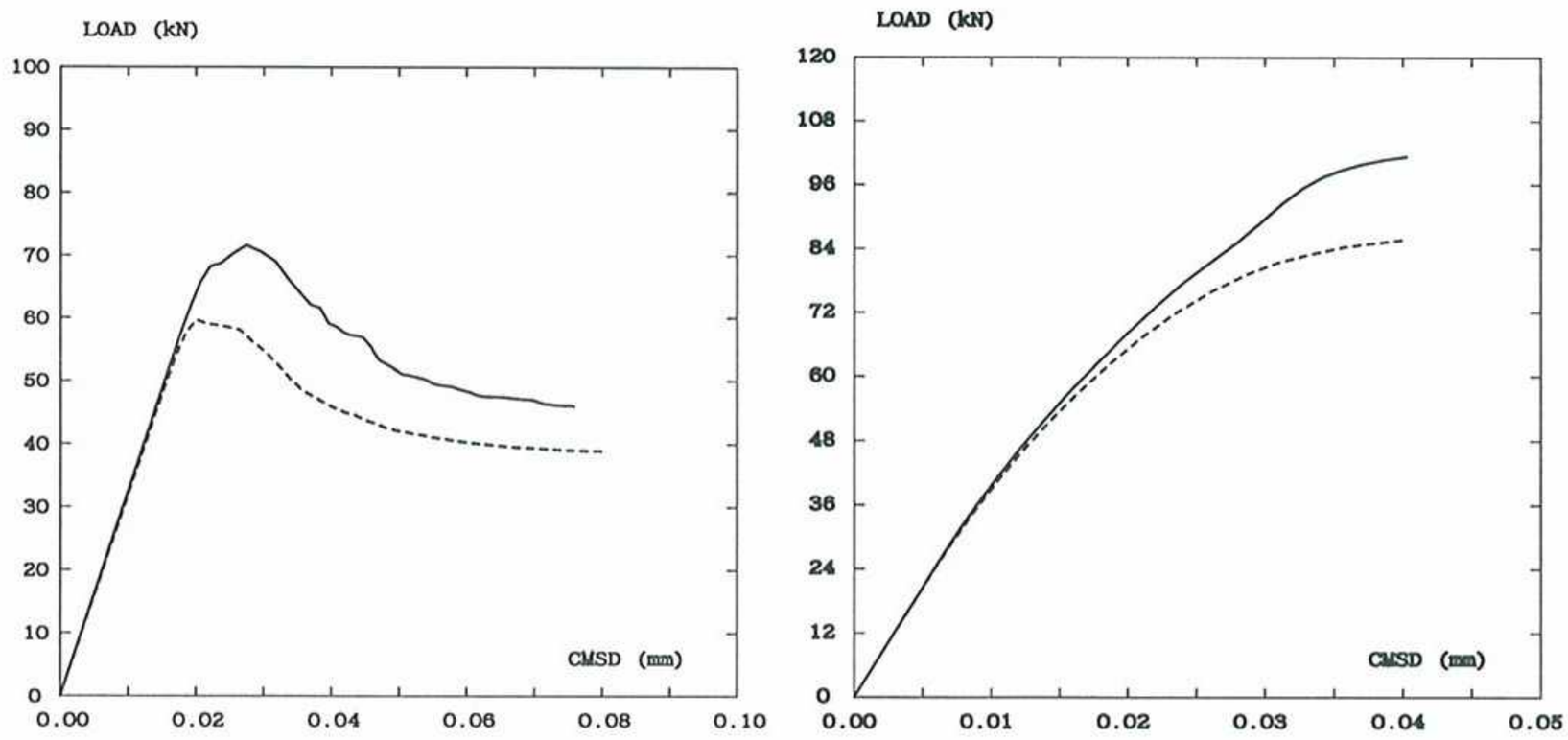

Figure 20. SENB test. Total load versus crack-mouth sliding displacement (CMSD) for meshes 0 (*solid line*) and 2 (*dashed line*): (**a**) with material 1 (large softening); (**b**) with material 2 (very slight softening)

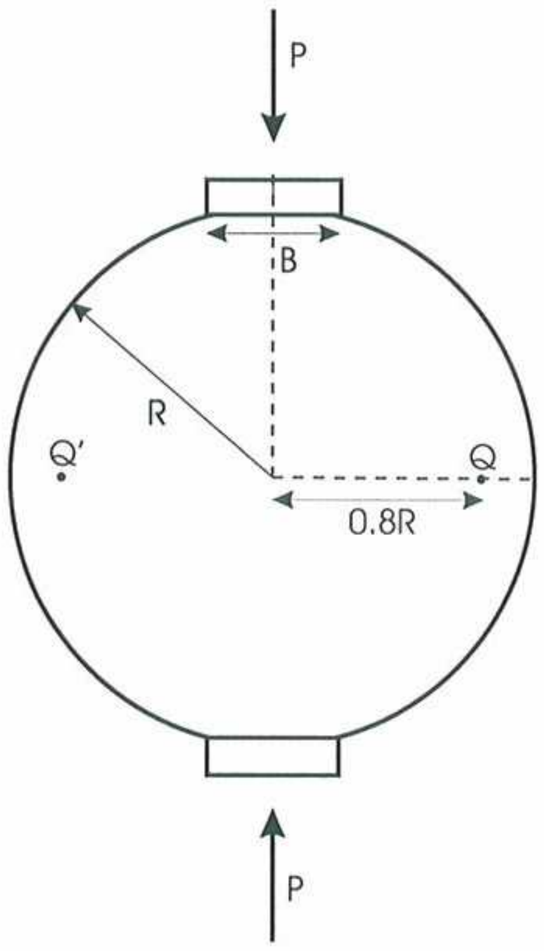

Figure 21. Brazilian test. Problem statement: specimen of radius R and bearing strip of width B. Points Q and Q' are used to define the Crack Opening Displacement (COD)

A plane strain analysis is carried out. The Mazars model is used for the quasi-brittle specimen, while the steel loading platens are assumed to be elastic. Geometrical and material parameters are shown in Table 9.

One goal of this example is to assess the influence of problem symmetry on the numerical results. For this reason, two different computational domains will be used, consisting of one-fourth and one-half of the problem domain, see Fig. 22.

Table 9
Brazilian test. Geometric and material parameters (Mazars model)

Meaning	**Symbol**	**Value**
Radius of specimen	R	40 mm
Width of bearing strip	B	10 mm
Young's modulus	E	37 700 MPa (specimen)
		300 000 MPa (bearing strip)
Poisson coefficient	ν	0.2
Characteristic length	l_c	2 mm
Damage threshold	Y_0	10^{-4}
Parameter A in compression	A_c	1.4
Parameter B in compression	B_c	1 900
Parameter A in tension	A_t	1
Parameter B in tension	B_t	15 600

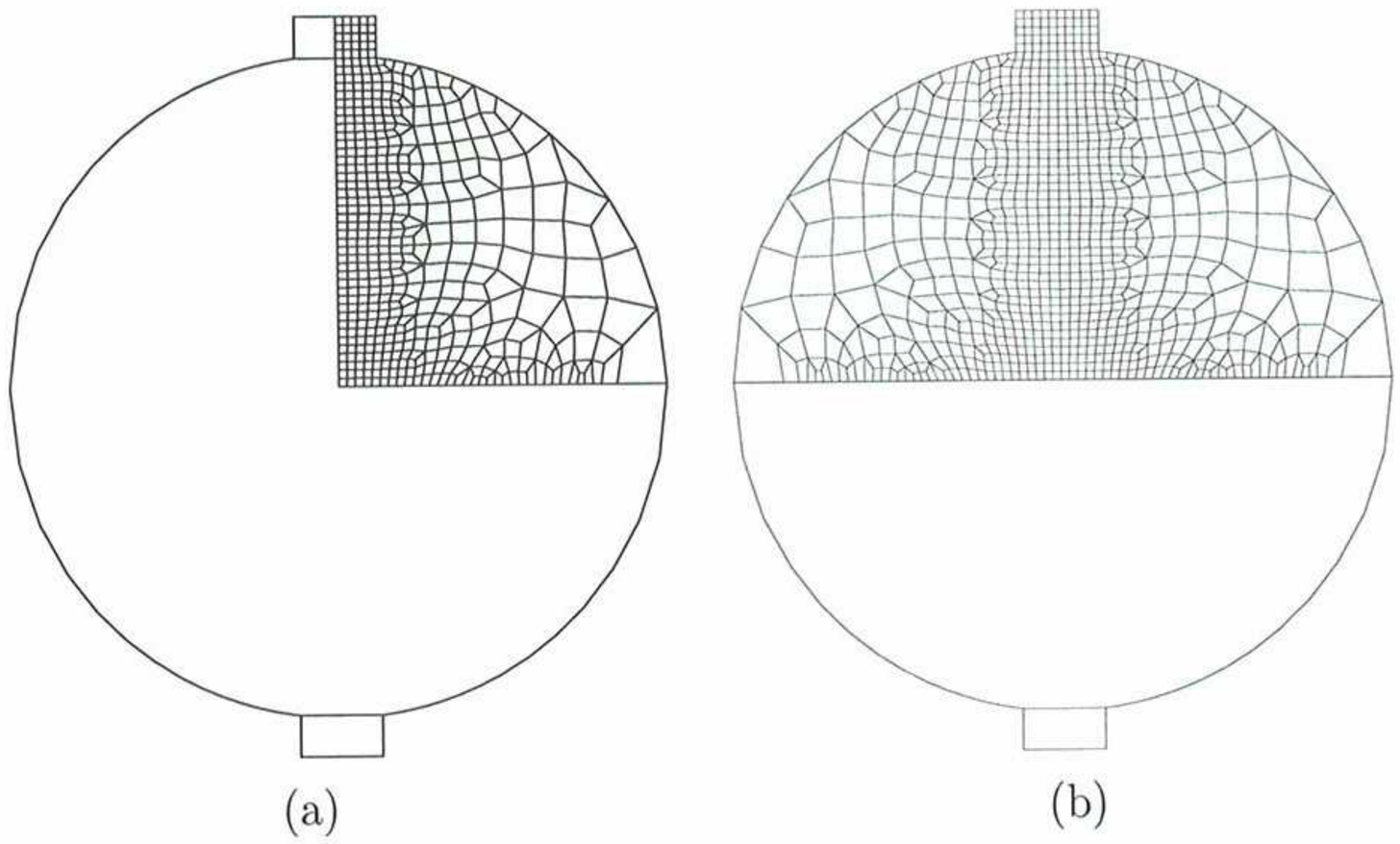

Figure 22. Brazilian test. Computational domain and finite element mesh for (**a**) one-fourth and (**b**) one-half of specimen

In both cases, adequate symmetry boundary conditions are prescribed along the symmetry axes, regarding both the displacement field and the nonlocal averaging.

Figure 23 depicts the structural response. The applied vertical load is plotted versus the vertical displacement of the bearing strip and versus the crack opening displacement (defined as the separation between points Q and Q', see Fig. 21 and [33].)

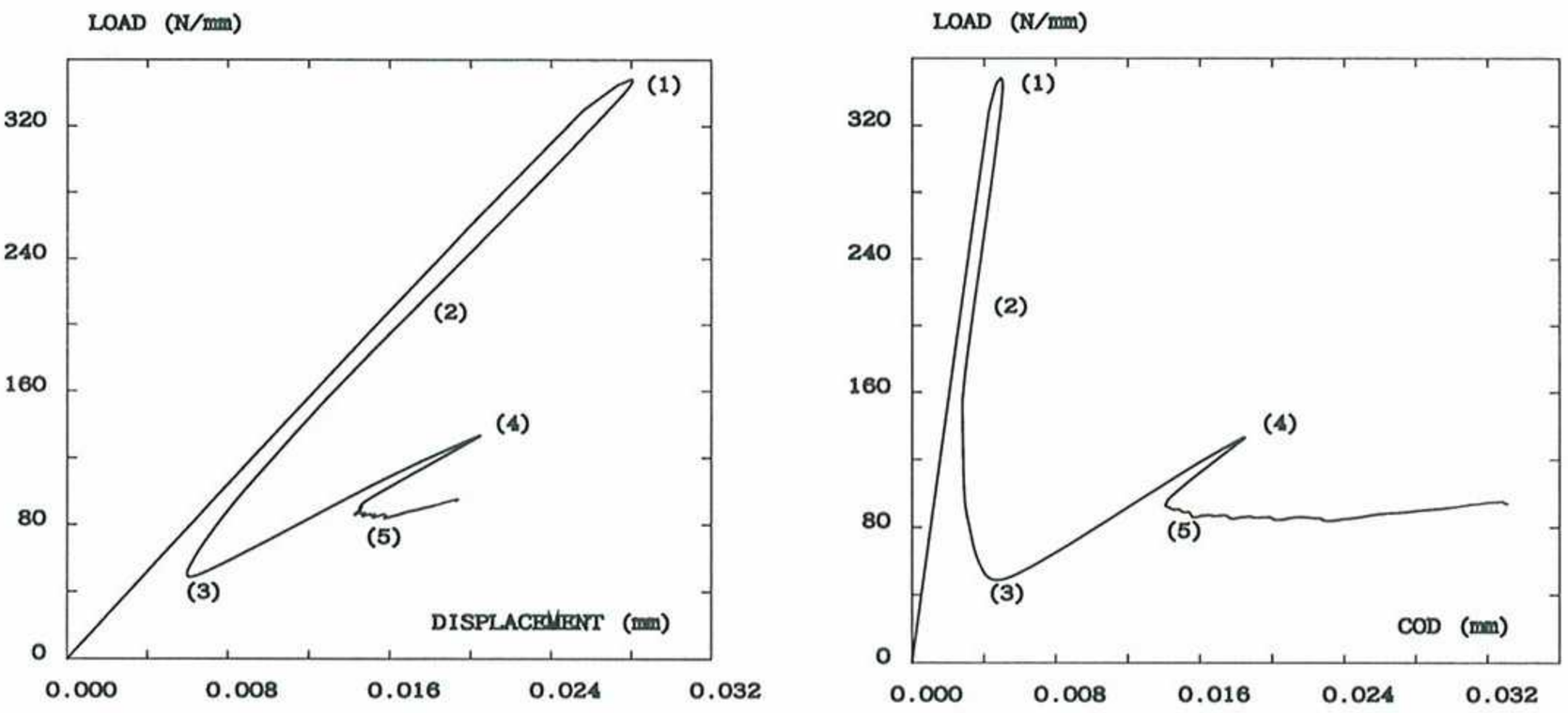

Figure 23. Brazilian test. Response with computational domain of Fig. 22(a). Load vs. (**a**) vertical displacement; (**b**) crack-opening displacement. Damage fields at states 1–5 depicted in Fig. 24

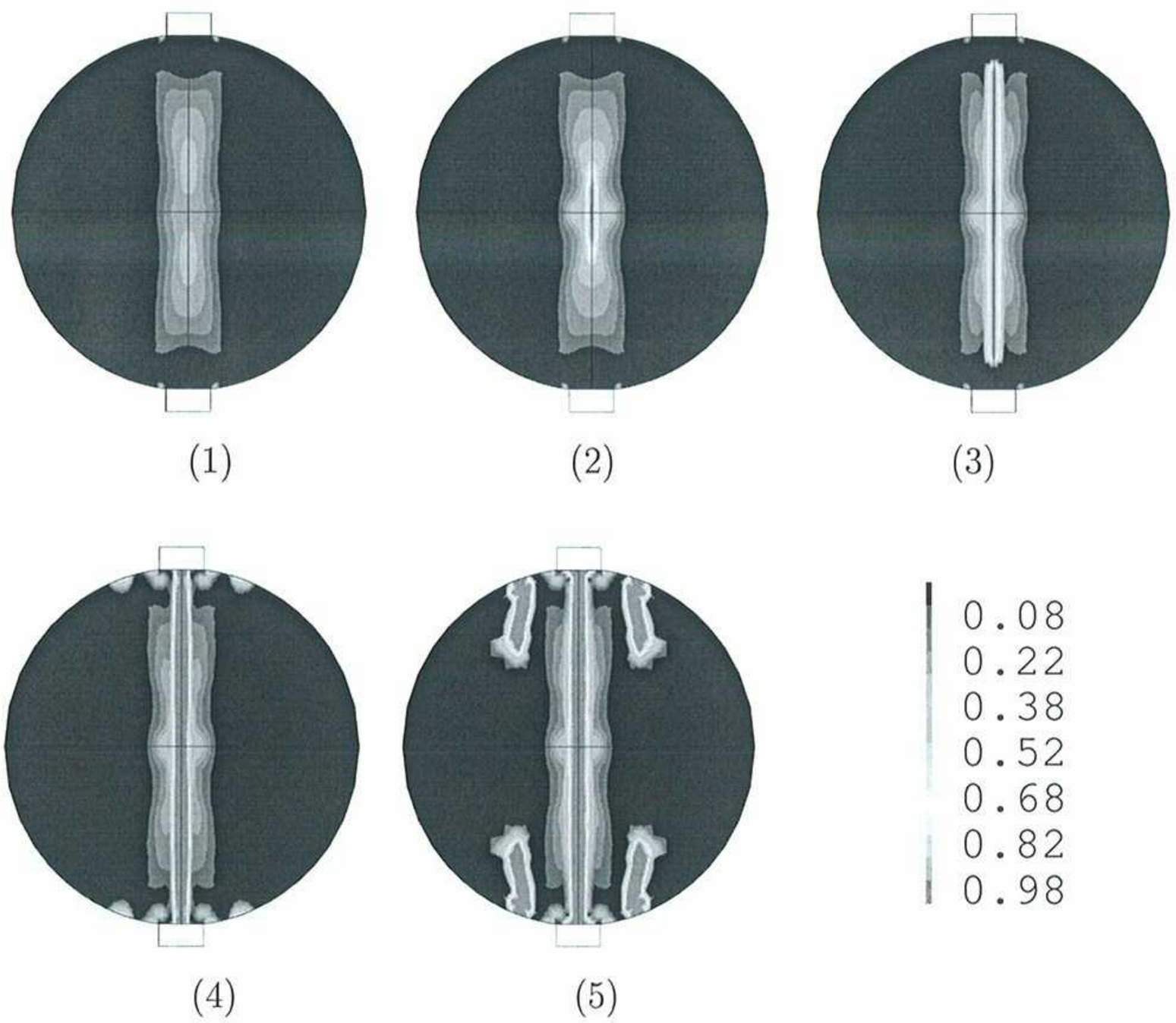

Figure 24. Brazilian test. Crack formation with computational domain of Fig. 22(a). Primary crack starts at centre of specimen and propagates outwards. Secondary cracks caused by compression on each half specimen resisting separately

The evolution of damage is depicted in Fig. 24. Damage starts above and below the centre of the specimen (state 1) and propagates along the loading plane (state 2) until it reaches the bearing plates (state 3). When this primary crack is fully developed, the specimen is split into two half discs. Under certain conditions, each half specimen has some extra resistance under compression. After some reloading (state 4, see Fig. 23), a secondary crack system leads finally to collapse. This complex failure pattern has been experimentally observed [33] and numerically analysed in detail in [34].

Note that the double symmetry in the crack system of Fig. 24 is prescribed a priori by the choice of the computational domain. However, one would not expect such a perfectly symmetrical behaviour in the actual experiment, especially considering the quasi-brittle nature of the material.

For this reason, the numerical test is repeated with one-half of the specimen as the computational domain, see Fig. 22(b). The evolution of damage is depicted in Fig. 25. As expected, the secondary crack is no longer symmetrical with respect to the vertical axis. Rounding errors (the numerical "equivalent" of material heterogeneity in the actual experiment) induce a slight non-symmetry in the primary crack and, as a result, the secondary crack only develops in one of the half discs.

The global structural behaviour is very similar for the two analyses, see Fig. 26. The force-displacement and force-COD curves only differ in the last part, which corresponds to the secondary crack. Note the larger stiffness of the solution with half specimen as computational domain, associated to the formation of the secondary crack in only one side.

6 Concluding Remarks

Efficiency and reliability are two crucial issues in any field of computational mechanics. We have addressed them here in the context of failure analysis of quasi-brittle materials by means of nonlocal damage models. The following conclusions may be pointed out:

- Advanced control strategies (displacement control or arc-length control with appropriate control variables) are needed to account in an efficient manner for the highly nonlinear and localized structural response.
- The consistent tangent matrix provides quadratic convergence in Newton equilibrium iterations. If the extra fill-in of this matrix caused by nonlocality is a critical factor, it can be avoided with an inner iterative loop.
- An adaptive strategy driven by an error estimator is required to ensure the quality of the numerical results in an objective manner.

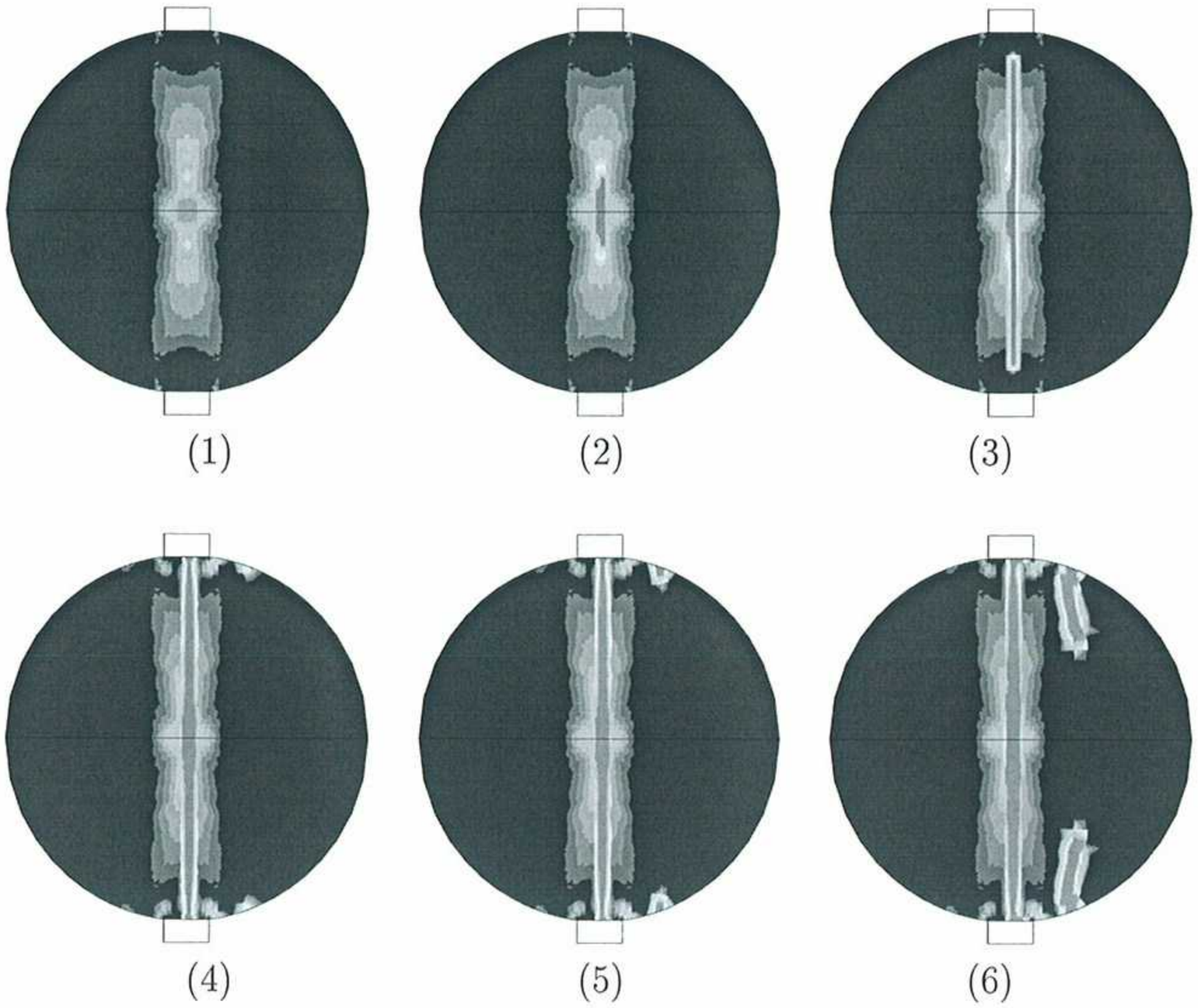

Figure 25. Brazilian test. Crack formation computed with one-half of the specimen as computational domain, see Fig. 22(b). Note that the secondary crack system is no longer symmetrical with respect to the vertical axis, cf. Fig. 24

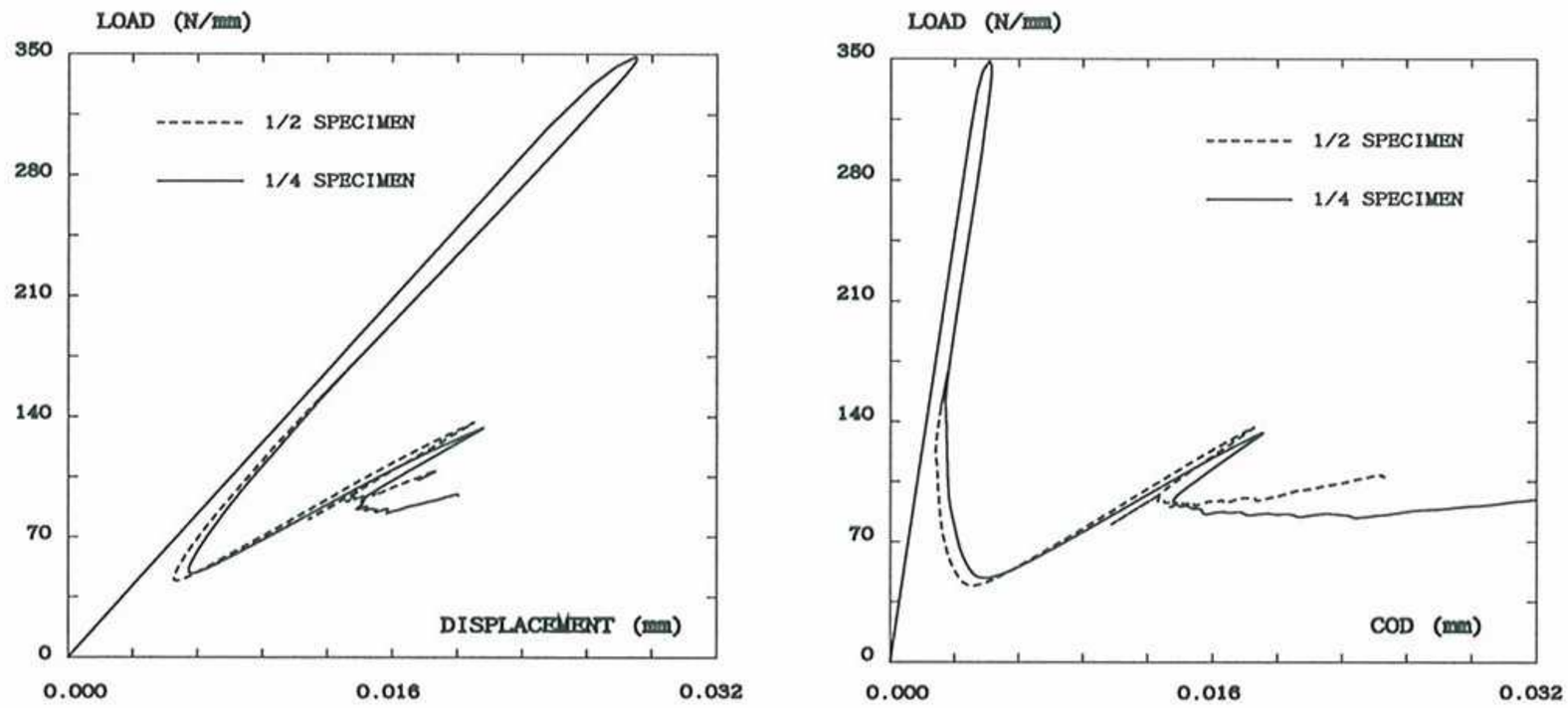

Figure 26. Brazilian test. Effect of computational domain on mechanical behaviour. Vertical load versus (**a**) vertical displacement; (**b**) crack-opening displacement

- The error estimator may be based on local computations – a common approach in residual-type error estimators –, provided that the damage model is slightly modified. The basic idea is that the *error* in the local state variable, rather than the variable itself, is averaged.

In the numerical examples, we have attempted to cover all relevant aspects, namely: the relative performance of various control strategies and nonlinear solvers (three-point bending test); the quantitative and qualitative influence of material parameters on structural response, assessed in an reliable way thanks to the error-estimator-driven adaptive strategy (single-edge notched beam test); the ability of the proposed approach to capture complex failure mechanisms and the role of symmetry in the computational domain (Brazilian test).

We have also briefly discussed a new nonlocal damage model based on the nonlocal average of displacements (rather than the state variable). Our preliminary results indicate that this model is sound from a physical point of view and has very attractive numerical properties, especially regarding the computation of the consistent tangent matrix.

References

[1] J. Lemaitre, J.-L. Chaboche, Mechanics of solid materials, Cambridge University Press, Cambridge, 1990.

[2] R. de Borst, J. Pamin, R. Peerlings, L. Sluys, On gradient-enhanced damage and plasticity models for failure in quasi-brittle and frictional materials, Comput. Mech. 17 (1–2) (1995) 130–141.

[3] G. Pijaudier-Cabot, Z. Bažant, Nonlocal damage theory, J. Eng. Mech.-ASCE 118 (10) (1987) 1512–1533.

[4] Z. Bažant, G. Pijaudier-Cabot, Nonlocal continuum damage, localization instability and convergence, J. Appl. Mech.-Trans. ASME 55 (2) (1988) 287–293.

[5] J. Mazars, G. Pijaudier-Cabot, Continuum damage theory – application to concrete, J. Eng. Mech.-ASCE 115 (2) (1989) 345–365.

[6] A. Rodríguez-Ferran, I. Arbós, A. Huerta, Adaptive analysis based on error estimation for nonlocal damage models, Revue européene des éléments finis 10 (2–4) (2001) 193–207.

[7] A. Rodríguez-Ferran, A. Huerta, Error estimation and adaptivity for nonlocal damage models, Int. J. Solids Struct. 37 (48–50) (2000) 7501–7528.

[8] M. Jirásek, B. Patzák, Consistent tangent stiffness for nonlocal damage models, Comput. Struct. 80 (14–15) (2002) 1279–1293.

[9] M. Jirásek, Nonlocal models for damage and fracture: comparison of approaches, Int. J. Solids Struct. 35 (31–32) (1998) 4133–4145.

[10] Z. Bažant, M. Jirásek, Nonlocal integral formulations of plasticity and damage: survey of progress, J. Eng. Mech.-ASCE 128 (11) (2002) 1119–1149.

[11] A. Huerta, G. Pijaudier-Cabot, Discretization influence on regularization by two localization limiters, J. Eng. Mech.-ASCE 120 (6) (1994) 1198–1218.

[12] J. Mazars, A description of micro- and macroscale damage of concrete structures, Eng. Fract. Mech. 25 (5–6) (1986) 729–737.

[13] J. de Vree, W. Brekelmans, M. van Gils, Comparison of nonlocal approaches in continuum damage mechanics, Comput. Struct. 55 (4) (1995) 581–588.

[14] J. Mazars, G. Pijaudier-Cabot, C. Saouridis, Size effect and continuous damage in cementitious materials, Int. J. Fract. 51 (2) (1991) 159–173.

[15] P. Pegon, A. Anthoine, Numerical strategies for solving continuum damage problems involving softening: application to the homogenization of masonry, in: Proceedings of the Second International Conference on Computational Structures Technology, Athens, 1994.

[16] H. Askes, L. Sluys, Remeshing strategies for adaptive ALE analysis of strain localisation, Eur. J. Mech. A-Solids 19 (3) (2000) 447–467.

[17] G. Pijaudier-Cabot, A. Huerta, Finite element analysis of bifurcation in nonlocal strain softening solids, Comput. Methods Appl. Mech. Eng. 90 (1–3) (1991) 905–919.

[18] P. Lancaster, K. Salkauskas, Surfaces generated by moving least squares methods, Math. Comput. 37 (155) (1981) 141–158.

[19] A. Huerta, S. Fernández-Méndez, Locking in the incompressible limit for the Element Free Galerkin method, Int. J. Numer. Methods Eng. 51 (11) (2001) 1361–1383.

[20] M. A. Crisfield, Non-linear finite element analysis of solids and structures. Volume 1: Essentials, John Wiley & Sons, Chichester, 1991.

[21] T. Belytschko, W. Liu, B. Moran, Nonlinear finite elements for continua and structures, John Wiley & Sons, Chichester, 2000.

[22] P. Díez, M. Arroyo, A. Huerta, Adaptive simulation of the coupled chemo-mechanical concrete degradation, in: H. Mang, F. Rammerstorfer, J. Eberhardsteiner (Eds.), Proceedings of the Fifth World Congress on Computational Mechanics (WCCM V), Vienna University of Technology, Austria, July 7-12, 2002, Vienna, Austria, http://wccm.tuwien.ac.at.

[23] C. Kelley, Iterative methods for linear and nonlinear equations, Vol. 16 of Frontiers in Applied Mathematics, Society for Industrial and Applied Mathematics, Philadelphia, 1995.

[24] A. Huerta, P. Díez, Error estimation including pollution assessment for nonlinear finite element analysis, Comput. Methods Appl. Mech. Eng. 181 (1–3) (2000) 21–41.

[25] J. Sarrate, A. Huerta, Efficient unstructured quadrilateral mesh generation, Int. J. Numer. Methods Eng. 49 (10) (2000) 1327–1350.

[26] P. Díez, J. Egozcue, A. Huerta, A posteriori error estimation for standard finite element analysis, Comput. Methods Appl. Mech. Eng. 163 (1–4) (1998) 141–157.

[27] P. Díez, M. Arroyo, A. Huerta, Adaptivity based on error estimation for viscoplastic softening materials, Mech. Cohesive-Frict. Mater. 5 (2) (2000) 87–112.

[28] P. Díez, A. Huerta, Error estimation for adaptivity in assumed-strain models for linear and nonlinear shells, Comput. Mech. Submitted.

[29] C. L. Bellégo, Couplages chimie-mécanique dans les structures en béton attaquées per l'eau: étude expérimentale et analyse numérique, Ph.D. thesis, E.N.S. Cachan (February 2001).

[30] A. Vila, A. Rodríguez-Ferran, A. Huerta, A note on a numerical benchmark test: an axisymmetric shell under ring loads, Commun. Numer. Methods Eng. 13 (3) (1997) 181–192.

[31] A. Carpinteri, S. Valente, G. Ferrara, G. Melchiorri, Is mode II fracture energy a real material property?, Comput. Struct. 48 (3) (1993) 397–413.

[32] R. Peerlings, R. de Borst, W. Brekelmans, M. Geers, Gradient-enhanced damage modelling of concrete fracture, Mech. Cohesive-Frict. Mater. 3 (4) (1998) 323–342.

[33] C. Rocco, G. Guinea, J. Planas, M. Elices, Mechanisms of rupture in splitting tests, ACI Mater. J. 96 (1) (1999) 52–60.

[34] A. Rodríguez-Ferran, A. Huerta, Failure and post-failure modelling of the Brazilian test, in: W. Wall, K.-U. Bletzinger, K. Schweizerhof (Eds.), Trends in Computational Structural Mechanics, CIMNE, Barcelona, 2001.